Simulated Annealing Optimization on Multi-Chamber Mufflers Hybridized with Perforated Plug-Inlet Under Space Constraints

Min-Chie CHIU

ChungChou Institute of Technology
Department of Automatic Control Engineering
6, Lane 2, Sec. 3, Shanchiao Rd., Yuanlin
Changhua 51003, Taiwan, R.O.C.
e-mail: minchie.chiu@msa.hinet.net

Because of the precious space in modern industry, a prerequisite in optimizing the acoustical performance of mufflers within a compact volume is necessary. To depress the acoustical performance, a multi-chamber muffler hybridized with perforated plug-inlet tubes which may dramatically increase the acoustical performance, is then adopted and optimized under space constraint.

In this paper, both the numerical decoupling technique and simulated annealing (*SA*) algorithm for solving the coupled acoustical problem of perforated plug-inlet tubes and optimizing the muffler shape are used. To appreciate the acoustical ability of the new mufflers, traditional multi-chamber mufflers with extended inlet tubes have been assessed. Furthermore, noise reductions in broadband and pure tones noise are also introduced. But before the *SA* operation can be carried out, the accuracy of the mathematical model has to be checked by experimental data. Results reveal that the maximal *STL* is precisely located at the desired target tone. In addition, the acoustical performance of mufflers conjugated with perforated plug-inlet tubes is superior to that hybridized with extended inlet tubes. Moreover, the more chambers the mufflers have, the higher acoustical performance they will reach. Consequently, we demonstrate a successful SA application to the muffler design.

Keywords: multi-chamber muffler, perforated plug-inlet tube, numerical decoupling technique, space constraints, SA optimization.

Notations

This paper is constructed on the basis of the following notations:

C_o – sound speed (m s^{-1}),

c_1, c_2 – coefficients of $\begin{matrix} p_2 \\ \rho_o c_o u_2 \end{matrix} = \begin{bmatrix} e^{-jk^+L} & e^{+jk^-L} \\ e^{-jk^+L} & -e^{+jk^-L} \end{bmatrix} \begin{matrix} c_1 \\ c_2 \end{matrix}$,

$C_{1,m,n}$, $C_{2,m,n}$ – coefficients with respect to the fundamental mode of m and n,

C_v – specific heat at constant volume (kJ kg^{-1} °K),

dh – diameter of perforated holes on the inner tube (m),

D_i – diameter of the i-th tube (m),

D_o – maximum diameter of the muffler (m),

f – cyclic frequency (Hz),

$Iter$ – maximum iteration,

j – imaginary unit,

J_m – Bessel function of order m,

kk – cooling rate in SA,

k – wave number ($= \omega/c_o$),

f_1, f_2, f_3, f_4 – coefficients of $\Gamma_i = f_i e^{\lambda_i x}$,

K_e – stagnation pressure loss factor between nodes 2&4 and nodes 7&9,

$k_{r,m,n}^{\pm}$ – wave number in r-direction,

L_i – lengths of i-th ducts (m),

L_A, L_B – lengths of the non-perforated segments in the plug-inlet tube (m),

L_C – length of the perforated segment in the plug-inlet tube (m),

L_o – total length of the muffler (m),

L_Z – length of the expansion chamber (m),

L_{Z-i} – length of the i-th segment duct (m),

M_i – mean flow Mach number at i-th node ($= V/C_o$),

OBJ_i – objective function,

$pb(T)$ – transition probability,

$p_{c,i}$ – aeroacoustic pressure at i-th node (Pa),

p_i – acoustic pressure at i-th node (Pa),

p_o – pressure of steady flow (Pa),

Q – volume flow rate of venting gas (m^{3}s^{-1}),

R – gas constant,

r, θ, z – axis of cylindrical coordinates,

S_i – section area at i-th node (m^2),

STL – sound transmission loss (dB),

SWL_i – the silenced SWL at silencer outlet at i-th octave band frequency,

SWL_T – the overall silenced SWL at silencer outlet,

$SWLO_i$ – the original SWL at silencer inlet at i-th octave band frequency,

t – the thickness of an inner perforated tube (m),

T_{ij} – components of a four-pole transfer system matrix,

TCE_{ij} – components of a four-pole transfer matrix for a simple contract/expansion duct,

TPE_{ij} – components of a four-pole transfer matrix for a perforated plug-inlet duct,

TS_{ij} – components of four-pole transfer matrices for straight ducts,

TE_{ij} – components of four-pole transfer matrices for extended ducts,

u – acoustical particle velocity in a perforated hole,

u_i – acoustic particle velocity at i-th node (m s^{-1}),

$\nu_{c,i}$ – vaeroacoustic mass velocity at i-th node (kg s^{-1}),

ν_i – acoustic mass velocity at i-th node (kg s^{-1}),

V – uniform velocity in the pipe ($V = Q/S_i$),

Y_i – characteristic impedance at i-th node ($Y_i = c_o/S_i$),

ρ_o – air density of steady flow (kg m^{-3}),

ρ_i – fluctuated density at i-th node (kg m^{-3}),

ς – specific acoustical impedance of a perforated tube,

η – the porosity of the perforated tube,

λ_i – i-th eigenvalue of $[\Psi]$,
γ – specific heat ratio of air,
$[\Omega]_{4\times4}$ – the model matrix formed by an eigenvector $\Omega_{4\times1}$ of $[\Psi]_{4\times4}$.

1. Introduction

In dealing with industrial flowing noise which is emitted from a venting system, a reactive muffler is customarily used [1]. As the space-constrained problem is mostly concerned with the necessity of operation and maintenance in practical engineering work, there is a growing need to optimize the acoustical performance under a limited space.

To increase the acoustical performance, the assessment of a new acoustical element – an internally perforated tube – was introduced and discussed by SULLIVAN and CROCKER in 1978 [2]. Based on the coupled equations derived by SULLIVAN and CROCKER in 1978 [2], a series of theories and numerical techniques in decoupling the acoustical problems have been proposed [3–7]. Concerning the flowing effect, MUNJAL [8] and PEAT [9] introduced the generalized decoupling and numerical decoupling methods in 1987 and 1988. However, the application of multi-chamber perforated plug-inlet tube mufflers within a space-constrained situation is rarely tackled.

In a previous work, the shape optimization of one-chamber mufflers conjugated with extended tubes has been discussed by CHANG *et al.* [10]. In order to appreciate the space-constrained multi-chamber perforated and plug-inlet tube mufflers used in eliminating industrial venting noise, two kinds of plug-inlet mufflers – a one-chamber and a two-chamber muffler conjugated with perforated and plug-inlet tubes – are proposed and investigated individually. Additionally, to distinguish the acoustical efficiency of a perforated and plug-inlet duct, the acoustical performance of a multi-chamber muffler hybridized with non-perforated and extended inlet tubes under the same space-constrained condition has also been discussed.

By adjusting the muffler's shape and using the simulated annealing (*SA*) method [11] and numerical decoupling methods, the optimal acoustical performances of mufflers can be achieved. Here, to achieve the optimal shape of mufflers, the *SA* method, a stochastic relaxation technique oriented by METROPOLIS *et al.* [12] and developed by KIRKPATRICK *et al.* [13] that imitates the physical process of annealing the metal to reach the minimum energy state, is applied in this work.

2. Mathematical models

In this paper, four kinds of mufflers hybridized with plug/non-plug inlet tubes in 1–2 chambers were adopted for the noise elimination in the constrained blower room shown in Fig. 1.
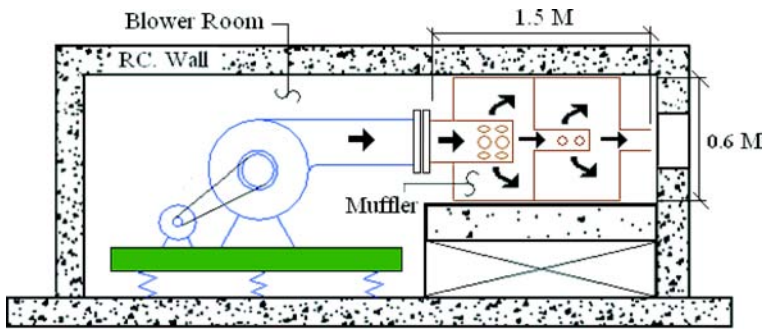
Fig. 1. The space-constrained blower room.

The outlines of these mufflers selected as the noise-reduction devices are shown in Figs. 2–5.
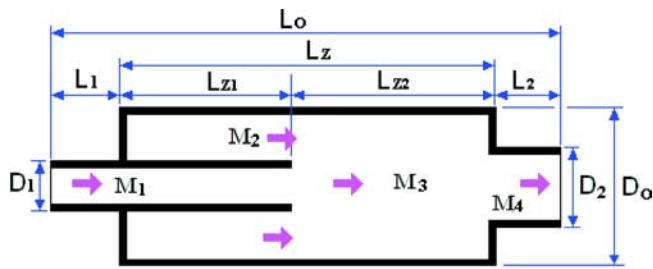

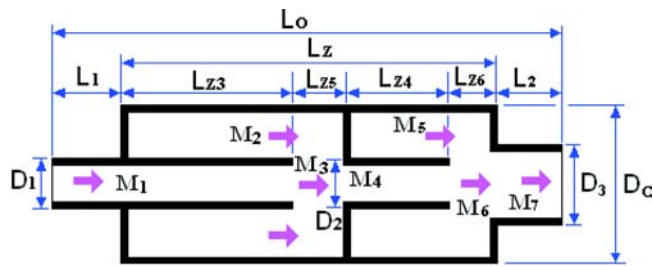Fig. 2. The outline of a one-chamber muffler hybridized with an extended inlet tube.

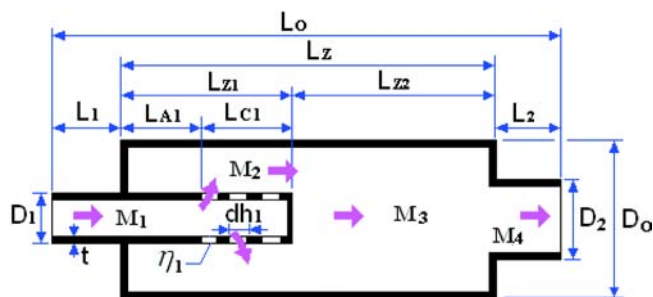Fig. 3. The outline of a two-chamber muffler hybridized with extended inlet tubes.

Fig. 4. The outline of a one-chamber muffler hybridized with a perforated plug-inlet tube.

Fig. 5. The outline of a two-chamber muffler hybridized with perforated plug-inlet tubes.

In addition, the recognitions of acoustical elements with respect to various mufflers are shown in Figs. 6–9. As indicated in Figs. 6 and 7, three kinds of muffler components, including straight duct, extended inlet duct, and simple contraction/expansion duct are recognized and denoted as I, II, and III.

Fig. 6. The recognition of acoustical elements for a one-chamber muffler hybridized with an extended inlet tube.

Fig. 7. The recognition of acoustical elements for a two-chamber muffler hybridized with extended inlet tubes.

Fig. 8. The recognition of acoustical elements for a one-chamber muffler hybridized with a perforated plug-inlet tube.
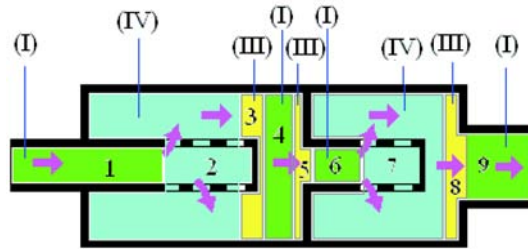
Fig. 9. The recognition of acoustical elements for a two-chamber muffler hybridized with perforated plug-inlet tubes.

Likewise, as indicated in Figs. 8 and 9, three kinds of muffler components, including straight duct, simple contraction/expansion duct, and perforated plug-inlet duct, are recognized and denoted as I, III, and IV. In Fig. 6, the one-chamber muffler system hybridized with an extended inlet tube is composed of five acoustical elements. Their related acoustic pressure p and acoustic particle velocity u in the acoustical field are represented by seven nodes and shown in Fig. 10.
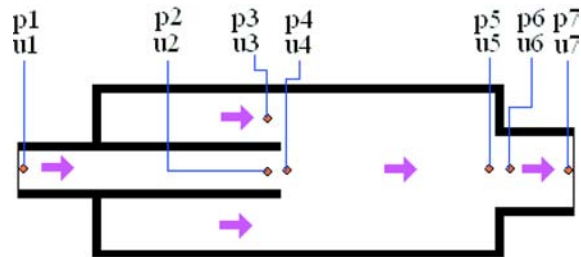

Fig. 10. The acoustical field in a one-chamber muffler hybridized with an extended inlet tube.

As indicated in Fig. 11, the related acoustic pressure p and acoustic particle velocity u in the acoustical field of a two-chamber muffler system hybridized with extended tubes are represented by twelve nodes.
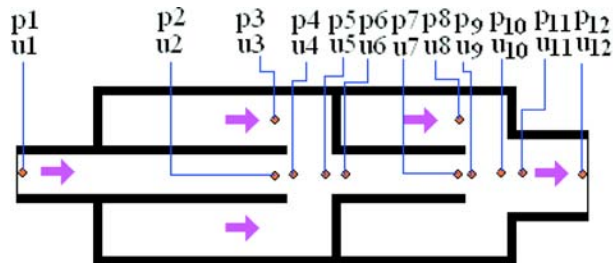

Fig. 11. The acoustical field in a two-chamber muffler hybridized with extended inlet tubes.

Similarly, in Fig. 12, the related acoustic pressure p and acoustic particle velocity u in the acoustical field of a one-chamber muffler system hybridized with a perforated plug-inlet tube are represented by seven nodes.
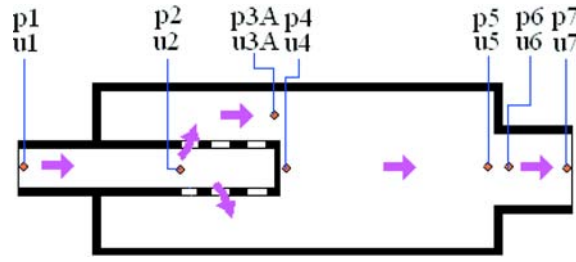
Fig. 12. The acoustical field in a one-chamber muffler hybridized with a perforated plug-inlet tube.

Consequently, as indicated in Fig. 13, the related acoustic pressure p and acoustic particle velocity u in the acoustical field of a two-chamber muffler system hybridized with perforated plug inlet tubes, are represented by twelve nodes.
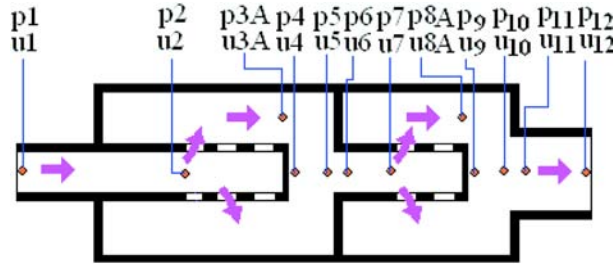

Fig. 13. The acoustical field in a two-chamber muffler hybridized with perforated plug-inlet tubes.

2.1. A one-chamber muffler hybridized with an extended inlet tube

The outlet of muffler is assumed under the free field circumstance (without reflection effect). As derived in the Appendices A and B, individual transfer matrices with respect to each case of a straight duct (I), an extended tube (II) and a simple contracted tube (III) [14, 15], are described as follows:

$$\begin{pmatrix} p_1 \\ \rho_o c_o u_1 \end{pmatrix} = e^{-jM_1 k(L_{Z1}+L_1)/(1-M_1^2)} \begin{bmatrix} TS11_{1,1} & TS11_{1,2} \\ TS11_{2,1} & TS11_{2,2} \end{bmatrix} \begin{pmatrix} p_2 \\ \rho_o c_o u_2 \end{pmatrix}, \quad (1)_1$$

$$TS11_{1,1} = \cos\left[\frac{k(L_{Z1}+L_1)}{1-M_1^2}\right], \qquad TS11_{1,2} = j\sin\left[\frac{k(L_{Z1}+L_1)}{1-M_1^2}\right],$$

$$(1)_2$$

$$TS11_{2,1} = j\sin\left[\frac{k(L_{Z1}+L_1)}{1-M_1^2}\right], \qquad TS11_{2,2} = \cos\left[\frac{k(L_{Z1}+L_1)}{1-M_1^2}\right],$$

$$\begin{pmatrix} p_2 \\ \rho_o c_o u_2 \end{pmatrix} = \begin{bmatrix} TE11_{1,1} & TE11_{1,2} \\ TE11_{2,1} & TE11_{2,2} \end{bmatrix} \begin{pmatrix} p_4 \\ \rho_o c_o u_4 \end{pmatrix}, \quad (2)$$

$$\begin{pmatrix} p_4 \\ \rho_o c_o u_4 \end{pmatrix} = e^{-jM_3 k L_{Z2}/(1-M_3^2)} \begin{bmatrix} TS12_{1,1} & TS12_{1,2} \\ TS12_{2,1} & TS12_{2,2} \end{bmatrix} \begin{pmatrix} p_5 \\ \rho_o c_o u_5 \end{pmatrix}, \qquad (3)_1$$

$$TS12_{1,1} = \cos\left[\frac{kL_{Z2}}{1-M_3^2}\right], \qquad TS12_{1,2} = j\sin\left[\frac{kL_{Z2}}{1-M_3^2}\right],$$

$$(3)_2$$

$$TS12_{2,1} = j\sin\left[\frac{kL_{Z2}}{1-M_3^2}\right], \qquad TS12_{2,2} = \cos\left[\frac{kL_{Z2}}{1-M_3^2}\right],$$

$$\begin{pmatrix} p_5 \\ \rho_o c_o u_5 \end{pmatrix} = \begin{bmatrix} TCE11_{1,1} & TCE11_{1,2} \\ TCE11_{2,1} & TCE11_{2,2} \end{bmatrix} \begin{pmatrix} p_6 \\ \rho_o c_o u_6 \end{pmatrix} \qquad (4)_1$$

$$TCE11_{1,1} = 1, \quad TCE11_{1,2} = 0, \quad TCE11_{2,1} = 0, \quad TCE11_{2,2} = \frac{S_6}{S_5}, \quad (4)_2$$

$$\begin{pmatrix} p_6 \\ \rho_o c_o u_6 \end{pmatrix} = e^{-jM_4 k L_2/(1-M_4^2)} \begin{bmatrix} TS13_{1,1} & TS13_{1,2} \\ TS13_{2,1} & TS13_{2,2} \end{bmatrix} \begin{pmatrix} p_7 \\ \rho_o c_o u_7 \end{pmatrix}, \qquad (5)_1$$

$$TS13_{1,1} = \cos\left[\frac{kL_2}{1-M_4^2}\right], \qquad TS13_{1,2} = j\sin\left[\frac{kL_2}{1-M_4^2}\right],$$

$$(5)_2$$

$$TS13_{2,1} = j\sin\left[\frac{kL_2}{1-M_4^2}\right], \qquad TS13_{2,2} = \cos\left[\frac{kL_2}{1-M_4^2}\right].$$

The total transfer matrix assembled by multiplication is

$$\begin{pmatrix} p_1 \\ \rho_o c_o u_1 \end{pmatrix} = e^{-jk\left[\frac{M_1(L_{Z1}+L_1)}{1-M_1^2} + \frac{M_3 L_{Z2}}{1-M_3^2} + \frac{M_4 L_2}{1-M_4^2}\right]}$$

$$\begin{bmatrix} TS11_{1,1} & TS11_{1,2} \\ TS11_{2,1} & TS11_{2,2} \end{bmatrix} \begin{bmatrix} TE11_{1,1} & TE11_{1,2} \\ TE11_{2,1} & TE11_{2,2} \end{bmatrix} \begin{bmatrix} TS12_{1,1} & TS12_{1,2} \\ TS12_{2,1} & TS12_{2,2} \end{bmatrix}$$

$$\begin{bmatrix} TCE11_{1,1} & TCE11_{1,2} \\ TCE11_{2,1} & TCE11_{2,2} \end{bmatrix} \begin{bmatrix} TS13_{1,1} & TS13_{1,2} \\ TS13_{2,1} & TS13_{2,2} \end{bmatrix} \begin{pmatrix} p_7 \\ \rho_o c_o u_7 \end{pmatrix}. \qquad (6)_1$$

A simplified form of the matrix is expressed as

$$\begin{pmatrix} p_1 \\ \rho_o c_o u_1 \end{pmatrix} = \begin{bmatrix} T_{11}^* & T_{12}^* \\ T_{21}^* & T_{22}^* \end{bmatrix} \begin{pmatrix} p_7 \\ \rho_o c_o u_7 \end{pmatrix}. \qquad (6)_2$$

The sound transmission loss (STL) of a muffler is defined as [14]

$$STL(Q, f, RT_1^{**}, RT_2^{**}, RT_3^{**}, RT_4^{**}, L_o, D_o)$$
$$= 20\log\left(\frac{|T_{11}^* + T_{12}^* + T_{21}^* + T_{22}^*|}{2}\right) + 10\log\left(\frac{S_1}{S_7}\right), \qquad (7)_1$$

where

$$L_o = L_1 + L_Z + L_2, \qquad L_Z = RT_1^{**} * L_o, \qquad L_{Z1} = RT_2^{**} * L_Z,$$

$$L_{Z2} = L_Z - L_{Z1}, \qquad L_2 = (L_o - L_Z)/2, \qquad D_1 = RT_3^{**} * D_o, \quad (7)_2$$

$$D_2 = RT_4^{**} * D_o.$$

2.2. A two-chamber muffler hybridized with extended inlet tubes

As described in Sec. 2.1, total transfer matrix of a two-chamber muffler hybridized with extended inlet tubes [14, 15] are described as

$$\begin{pmatrix} p_1 \\ \rho_o c_o u_1 \end{pmatrix} = e^{-jk\left[\frac{M_1(L_1+L_{Z1})}{1-M_1^2} + \frac{M_3 L_{Z5}}{1-M_3^2} + \frac{M_4 L_{Z4}}{1-M_4^2} + \frac{M_6 L_{Z6}}{1-M_6^2} + \frac{M_7 L_2}{1-M_7^2}\right]}$$

$$\begin{bmatrix} TS21_{1,1} & TS21_{1,2} \\ TS21_{2,1} & TS21_{2,2} \end{bmatrix} \begin{bmatrix} TE21_{1,1} & TE21_{1,2} \\ TE21_{2,1} & TE21_{2,2} \end{bmatrix} \begin{bmatrix} TS22_{1,1} & TS22_{1,2} \\ TS22_{2,1} & TS22_{2,2} \end{bmatrix}$$

$$\begin{bmatrix} TCE21_{1,1} & TCE21_{1,2} \\ TCE21_{2,1} & TCE21_{2,2} \end{bmatrix} \begin{bmatrix} TS23_{1,1} & TS23_{1,2} \\ TS23_{2,1} & TS23_{2,2} \end{bmatrix} \begin{bmatrix} TE22_{1,1} & TE22_{1,2} \\ TE22_{2,1} & TE22_{2,2} \end{bmatrix}$$

$$\begin{bmatrix} TS24_{1,1} & TS24_{1,2} \\ TS24_{2,1} & TS24_{2,2} \end{bmatrix} \begin{bmatrix} TCE22_{1,1} & TCE22_{1,2} \\ TCE22_{2,1} & TCE22_{2,2} \end{bmatrix} \begin{bmatrix} TS25_{1,1} & TS25_{1,2} \\ TS25_{2,1} & TS25_{2,2} \end{bmatrix} \begin{pmatrix} p_{12} \\ \rho_o c_o u_{12} \end{pmatrix}, \quad (8)_1$$

where

$$TS21_{1,1} = \cos\left[\frac{k(L_{Z1}+L_1)}{1-M_1^2}\right], \qquad TS21_{1,2} = j\sin\left[\frac{k(L_{Z1}+L_1)}{1-M_1^2}\right],$$

$$TS21_{2,1} = j\sin\left[\frac{k(L_{Z1}+L_1)}{1-M_1^2}\right], \qquad TS21_{2,2} = \cos\left[\frac{k(L_{Z1}+L_1)}{1-M_1^2}\right],$$

$$TS22_{1,1} = \cos\left[\frac{kL_{Z5}}{1-M_3^2}\right], \qquad TS22_{1,2} = j\sin\left[\frac{kL_{Z5}}{1-M_3^2}\right],$$

$$TS22_{2,1} = j\sin\left[\frac{kL_{Z5}}{1-M_3^2}\right], \qquad TS22_{2,2} = \cos\left[\frac{kL_{Z5}}{1-M_3^2}\right], \qquad (8)_2$$

$$TCE21_{1,1} = 1, \qquad TCE21_{1,2} = 0,$$

$$TCE21_{2,1} = 0, \qquad TCE21_{2,2} = \frac{S_6}{S_5},$$

$$TS23_{1,1} = \cos\left[\frac{kL_{Z4}}{1-M_4^2}\right], \qquad TS23_{1,2} = j\sin\left[\frac{kL_{Z4}}{1-M_4^2}\right],$$

$$TS23_{2,1} = j\sin\left[\frac{kL_{Z4}}{1-M_4^2}\right], \qquad TS23_{2,2} = \cos\left[\frac{kL_{Z4}}{1-M_4^2}\right],$$

$$TS24_{1,1} = \cos\left[\frac{kL_{Z6}}{1-M_6^2}\right], \qquad TS24_{1,2} = j\sin\left[\frac{kL_{Z6}}{1-M_6^2}\right],$$

$$TS24_{2,1} = j\sin\left[\frac{kL_{Z6}}{1-M_6^2}\right], \qquad TS24_{2,2} = \cos\left[\frac{kL_{Z6}}{1-M_6^2}\right],$$

$$TCE22_{1,1} = 1, \qquad TCE22_{1,2} = 0,$$

$$TCE22_{2,1} = 0, \qquad TCE22_{2,2} = \frac{S_{11}}{S_{10}}, \qquad (8)_2 \text{ [cont.]}$$

$$TS25_{1,1} = \cos\left[\frac{kL_2}{1-M_7^2}\right], \qquad TS25_{1,2} = j\sin\left[\frac{kL_2}{1-M_7^2}\right],$$

$$TS25_{2,1} = j\sin\left[\frac{kL_2}{1-M_7^2}\right], \qquad TS25_{2,2} = \cos\left[\frac{kL_2}{1-M_7^2}\right].$$

A simplified form of the matrix is expressed as

$$\begin{pmatrix} p_1 \\ \rho_o c_o u_1 \end{pmatrix} = \begin{bmatrix} T_{11}^{**} & T_{12}^{**} \\ T_{21}^{**} & T_{22}^{**} \end{bmatrix} \begin{pmatrix} p_{12} \\ \rho_o c_o u_{12} \end{pmatrix}. \qquad (9)$$

The *STL* of a muffler is defined as [14]

$$STL(Q, f, RT_1^{***}, RT_2^{***}, RT_3^{***}, RT_4^{***}, RT_5^{***}, RT_6^{***}, RT_7^{***}, L_o, D_o)$$

$$= 20\log\left(\frac{|T_{11}^{**} + T_{12}^{**} + T_{21}^{**} + T_{22}^{**}|}{2}\right) + 10\log\left(\frac{S_1}{S_{12}}\right), \qquad (10)_1$$

where

$$L_o = L_1 + L_Z + L_2, \qquad L_Z = RT_1^{***} * L_o,$$

$$L_{Z1} = RT_2^{***} * L_Z, \qquad L_{Z2} = L_Z - L_{Z1},$$

$$L_{Z3} = RT_3^{***} * L_{Z1}, \qquad L_{Z5} = L_{Z1} - L_{Z3},$$

$$L_{Z4} = RT_4^{***} * L_{Z2}, \qquad L_{Z6} = L_{Z2} - L_{Z4}, \qquad (10)_2$$

$$L_2 = (L_o - L_Z)/2, \qquad D_1 = RT_5^{***} * D_o,$$

$$D_2 = RT_6^{***} * D_o, \qquad D_3 = RT_7^{***} * D_o.$$

2.3. A one-chamber muffler hybridized with a perforated plug-inlet tube

As derived in the Appendices A and C, total transfer matrix of a one-chamber muffler hybridized with a perforated plug-inlet tubes [14, 15] are described as

$$\begin{pmatrix} p_1 \\ \rho_o c_o u_1 \end{pmatrix} = e^{-jk\left[\frac{M_1(L_{A1}+L_1)}{1-M_1^2} + \frac{M_3 L_{Z2}}{1-M_3^2} + \frac{M_4 L_2}{1-M_4^2}\right]}$$

$$\begin{bmatrix} TS31_{1,1} & TS31_{1,2} \\ TS31_{2,1} & TS31_{2,2} \end{bmatrix} \begin{bmatrix} TPE31_{1,1} & TPE31_{1,2} \\ TPE31_{2,1} & TPE31_{2,2} \end{bmatrix} \begin{bmatrix} TCE31_{1,1} & TCE31_{1,2} \\ TCE32_{2,1} & TCE31_{2,2} \end{bmatrix}$$

$$\begin{bmatrix} TS32_{1,1} & TS32_{1,2} \\ TS32_{2,1} & TS32_{2,2} \end{bmatrix} \begin{bmatrix} TCE32_{1,1} & TCE32_{1,2} \\ TCE32_{2,1} & TCE32_{2,2} \end{bmatrix} \begin{bmatrix} TS33_{1,1} & TS33_{1,2} \\ TS33_{2,1} & TS33_{2,2} \end{bmatrix} \begin{pmatrix} p_7 \\ \rho_o c_o u_7 \end{pmatrix}, \quad (11)_1$$

where

$$TS31_{1,1} = \cos\left[\frac{k(L_{A1}+L_1)}{1-M_1^2}\right], \qquad TS31_{1,2} = j\sin\left[\frac{k(L_{A1}+L_1)}{1-M_1^2}\right],$$

$$TS31_{2,1} = j\sin\left[\frac{k(L_{A1}+L_1)}{1-M_1^2}\right], \qquad TS31_{2,2} = \cos\left[\frac{k(L_{A1}+L_1)}{1-M_1^2}\right],$$

$$TCE31_{1,1} = 1, \qquad TCE31_{1,2} = 0,$$

$$TCE31_{2,1} = 0, \qquad TCE31_{2,2} = \frac{S_4}{S_3},$$

$$TS32_{1,1} = \cos\left[\frac{kL_{Z2}}{1-M_3^2}\right], \qquad TS32_{1,2} = j\sin\left[\frac{kL_{Z2}}{1-M_3^2}\right],$$

$$TS32_{2,1} = j\sin\left[\frac{kL_{Z2}}{1-M_3^2}\right], \qquad TS32_{2,2} = \cos\left[\frac{kL_{Z2}}{1-M_3^2}\right], \qquad (11)_2$$

$$TCE32_{1,1} = 1, \qquad TCE32_{1,2} = 0,$$

$$TCE32_{2,1} = 0, \qquad TCE32_{2,2} = \frac{S_6}{S_5},$$

$$TS33_{1,1} = \cos\left[\frac{kL_2}{1-M_4^2}\right], \qquad TS33_{1,2} = j\sin\left[\frac{kL_2}{1-M_4^2}\right],$$

$$TS33_{2,1} = j\sin\left[\frac{kL_2}{1-M_4^2}\right], \qquad TS33_{2,2} = \cos\left[\frac{kL_2}{1-M_4^2}\right].$$

A simplified form in the matrix is expressed as

$$\begin{pmatrix} p_1 \\ \rho_o c_o u_1 \end{pmatrix} = \begin{bmatrix} T_{11}^{***} & T_{12}^{***} \\ T_{21}^{***} & T_{22}^{***} \end{bmatrix} \begin{pmatrix} p_7 \\ \rho_o c_o u_7 \end{pmatrix}. \qquad (12)$$

The *STL* of a muffler is defined as [14]

$$STL(Q, f, RT_1, RT_2, RT_3, RT_4, RT_5, RT_6, RT_7, L_o, D_o)$$

$$= 20\log\left(\frac{|T_{11}^{***} + T_{12}^{***} + T_{21}^{***} + T_{22}^{***}|}{2}\right) + 10\log\left(\frac{S_1}{S_7}\right), \qquad (13)_1$$

where

$$L_o = L_1 + L_Z + L_2, \qquad L_Z = RT_1^* L_o,$$

$$L_{Z1} = RT_2^* L_Z, \qquad L_{Z2} = L_Z - L_{Z1},$$

$$L_2 = (L_o - L_Z)/2, \qquad D_1 = RT_3^* D_o,$$

$$D_2 = RT_4^* D_o, \qquad L_{C1} = RT_5^* L_{Z1}, \qquad (13)_2$$

$$\eta_1 = RT_6, \qquad DH_1 = RT_7.$$

2.4. A two-chamber muffler hybridized with perforated plug inlet tubes

Similarly, as described in Sec. 2.3, total transfer matrix of a two-chamber muffler hybridized with a perforated plug-inlet tubes [14, 15] are described as

$$\begin{pmatrix} p_1 \\ \rho_o c_o u_1 \end{pmatrix} = e^{-jk\left[\frac{M_1(L_{A1}+L_1)}{1-M_1^2} + \frac{M_3 L_{Z5}}{1-M_3^2} + \frac{M_4 L_{A2}}{1-M_4^2} + \frac{M_6 L_{Z6}}{1-M_6^2} + \frac{M_7 L_2}{1-M_7^2}\right]}$$

$$\begin{bmatrix} TS41_{1,1} & TS41_{1,2} \\ TS41_{2,1} & TS41_{2,2} \end{bmatrix} \begin{bmatrix} TPE41_{1,1} & TPE41_{1,2} \\ TPE41_{2,1} & TPE41_{2,2} \end{bmatrix} \begin{bmatrix} TCE41_{1,1} & TCE41_{1,2} \\ TCE42_{2,1} & TCE41_{2,2} \end{bmatrix}$$

$$\begin{bmatrix} TS42_{1,1} & TS42_{1,2} \\ TS42_{2,1} & TS42_{2,2} \end{bmatrix} \begin{bmatrix} TCE42_{1,1} & TCE42_{1,2} \\ TCE42_{2,1} & TCE42_{2,2} \end{bmatrix} \begin{bmatrix} TS43_{1,1} & TS43_{1,2} \\ TS43_{2,1} & TS43_{2,2} \end{bmatrix}$$

$$\begin{bmatrix} TPE42_{1,1} & TPE42_{1,2} \\ TPE42_{2,1} & TPE42_{2,2} \end{bmatrix} \begin{bmatrix} TCE43_{1,1} & TCE43_{1,2} \\ TCE43_{2,1} & TCE43_{2,2} \end{bmatrix} \begin{bmatrix} TS44_{1,1} & TS44_{1,2} \\ TS44_{2,1} & TS44_{2,2} \end{bmatrix}$$

$$\begin{bmatrix} TCE44_{1,1} & TCE44_{1,2} \\ TCE44_{2,1} & TCE44_{2,2} \end{bmatrix} \begin{bmatrix} TS45_{1,1} & TS45_{1,2} \\ TS45_{2,1} & TS45_{2,2} \end{bmatrix} \begin{pmatrix} p_{12} \\ \rho_o c_o u_{12} \end{pmatrix}, \quad (14)_1$$

where

$$TS41_{1,1} = \cos\left[\frac{k(L_{A1}+L_1)}{1-M_1^2}\right], \qquad TS41_{1,2} = j\sin\left[\frac{k(L_{A1}+L_1)}{1-M_1^2}\right],$$

$$TS41_{2,1} = j\sin\left[\frac{k(L_{A1}+L_1)}{1-M_1^2}\right], \qquad TS41_{2,2} = \cos\left[\frac{k(L_{A1}+L_1)}{1-M_1^2}\right],$$

$$TCE41_{1,1} = 1, \qquad\qquad TCE41_{1,2} = 0,$$

$$TCE41_{2,1} = 0, \qquad\qquad TCE31_{2,2} = \frac{S_4}{S_3}, \qquad (14)_2$$

$$TS42_{1,1} = \cos\left[\frac{kL_{Z5}}{1-M_3^2}\right], \qquad TS42_{1,2} = j\sin\left[\frac{kL_{Z5}}{1-M_3^2}\right],$$

$$TS42_{2,1} = j\sin\left[\frac{kL_{Z5}}{1-M_3^2}\right], \qquad TS42_{2,2} = \cos\left[\frac{kL_{Z5}}{1-M_3^2}\right],$$

$$TCE42_{1,1} = 1, \qquad\qquad TCE42_{1,2} = 0,$$

$$TCE42_{2,1} = 0, \qquad\qquad TCE42_{2,2} = \frac{S_6}{S_5},$$

$$TS43_{1,1} = \cos\left[\frac{kL_{A2}}{1 - M_4^2}\right], \qquad TS43_{1,2} = j\sin\left[\frac{kL_{A2}}{1 - M_4^2}\right],$$

$$TS43_{2,1} = j\sin\left[\frac{kL_{A2}}{1 - M_4^2}\right], \qquad TS43_{2,2} = \cos\left[\frac{kL_{A2}}{1 - M_4^2}\right],$$

$$TCE43_{1,1} = 1, \qquad\qquad TCE43_{1,2} = 0,$$

$$TCE43_{2,1} = 0, \qquad\qquad TCE33_{2,2} = \frac{S_9}{S_8},$$

$$TS44_{1,1} = \cos\left[\frac{kL_{Z6}}{1 - M_6^2}\right], \qquad TS44_{1,2} = j\sin\left[\frac{kL_{Z6}}{1 - M_6^2}\right], \qquad \begin{matrix}(14)_2 \\ \text{[cont.]}\end{matrix}$$

$$TS44_{2,1} = j\sin\left[\frac{kL_{Z6}}{1 - M_6^2}\right], \qquad TS44_{2,2} = \cos\left[\frac{kL_{Z6}}{1 - M_6^2}\right],$$

$$TCE44_{1,1} = 1, \qquad\qquad TCE44_{1,2} = 0,$$

$$TCE44_{2,1} = 0, \qquad\qquad TCE44_{2,2} = \frac{S_{11}}{S_{10}},$$

$$TS45_{1,1} = \cos\left[\frac{kL_2}{1 - M_7^2}\right], \qquad TS45_{1,2} = j\sin\left[\frac{kL_2}{1 - M_7^2}\right],$$

$$TS45_{2,1} = j\sin\left[\frac{kL_2}{1 - M_7^2}\right], \qquad TS45_{2,2} = \cos\left[\frac{kL_2}{1 - M_7^2}\right].$$

A simplified form of the matrix is expressed as

$$\begin{pmatrix} p_1 \\ \rho_o c_o u_1 \end{pmatrix} = \begin{bmatrix} T_{11}^{****} & T_{12}^{****} \\ T_{21}^{****} & T_{22}^{****} \end{bmatrix} \begin{pmatrix} p_{12} \\ \rho_o c_o u_{12} \end{pmatrix}. \tag{15}$$

The *STL* of a muffler is defined as [14]

$$STL(Q, f, RT_1^*, RT_2^*, RT_3^*, RT_4^*, RT_5^*, RT_6^*, RT_7^*, RT_8^*, RT_9^*, RT_{10}^*, RT_{11}^*,$$

$$RT_{12}^*, RT_{13}^*, L_o, D_o) = 20\log\left(\frac{|T_{11}^{****} + T_{12}^{****} + T_{21}^{****} + T_{22}^{****}|}{2}\right)$$

$$+ 10\log\left(\frac{S_1}{S_{12}}\right), \tag{16$_1$}$$

where

$$L_o = L_1 + L_Z + L_2, \qquad L_Z = RT_1^* * L_o,$$

$$L_{Z1} = RT_2^* * L_Z, \qquad L_{Z2} = L_Z - L_{Z1},$$

$$L_{Z3} = RT_3^* * L_{Z1}, \qquad L_{Z5} = L_{Z1} - L_{Z3},$$

$$L_2 = (L_o - L_Z)/2, \qquad L_{C1} = RT_4^* * L_{Z3},$$

$$L_{A1} = L_{Z3} - L_{C1}, \qquad DH_1 = RT_5^*,$$

$$L_{Z4} = RT_6^* * L_{Z2}, \qquad L_{Z6} = L_{Z2} - L_{Z4}, \qquad (16)_2$$

$$L_{C2} = RT_7^* * L_{Z4}, \qquad L_{A2} = L_{Z4} - L_{C2},$$

$$DH_2 = RT_8^*, \qquad D_1 = RT_9^* * D_o,$$

$$D_2 = RT_{10}^* * D_o, \qquad D_3 = RT_{11}^* * D_o,$$

$$\eta_1 = RT_{12}^*, \qquad \eta_2 = RT_{13}^*.$$

2.5. Overall sound power level

The silenced octave sound power level emitted from a muffler's outlet is

$$SWL_i = SWLO_i - STL_i \qquad (17)$$

where
1. $SWLO_i$ is the original SWL at inlet of the muffler (or pipe outlet), and i is the index of the octave band frequency.
2. STL_i is the muffler's STL with respect to the relative octave band frequency.
3. SWL_i is the silenced SWL at the outlet of the muffler with respect to the relative octave band frequency.

Finally, the overall SWL_T silenced by the muffler at the outlet is

$$SWL_T = 10 * \log \left\{ \sum_{i=1}^{5} 10^{SWL_i/10} \right\}$$

$$= 10 * \log \left\{ \begin{array}{l} 10^{[SWLO(f=125) - STL(f=125)]/10} + 10^{[SWLO(f=250) - STL(f=250)]/10} \\ \\ + 10^{[SWLO(f=500) - STL(f=500)]/10} + 10^{[SWLO(f=1000) - STL(f=1000)]/10} + 10^{[SWLO(f=2000) - STL(f=2000)]/10} \end{array} \right\}. \qquad (18)$$

2.6. Objective function

By using the formulas of Eqs. (7), (10), (13), (16), the objective function used in the SA optimization with respect to each type of muffler was established.

For the type of one-chamber muffler with an extended inlet tube, the objective function in maximizing the STL at pure tone (f) is

$$OBJ_{11} = STL(Q, f, RT_1^{**}, RT_2^{**}, RT_3^{**}, RT_4^{**}, L_o, D_o)$$
$$= 20 \log \left(\frac{|T_{11}^* + T_{12}^* + T_{21}^* + T_{22}^*|}{2} \right) + 10 \log \left(\frac{S_1}{S_7} \right). \qquad (19)$$

The objective function in minimizing the overall SWL is

$$OBJ_{12} = SWL_T(Q, RT_1^{**}, RT_2^{**}, RT_3^{**}, RT_4^{**}, L_o, D_o). \qquad (20)$$

Similarly, the objective functions (OBJ_{21}, OBJ_{22}) in maximizing the STL at the pure tone (f) and minimizing the overall SWL for a two-chamber with extended inlet tubes are

$$OBJ_{21} = STL(Q, f, RT_1^{***}, RT_2^{***}, RT_3^{***}, RT_4^{***}, RT_5^{***}, RT_6^{***}, RT_7^{***}, L_o, D_o)$$
$$= 20 \log \left(\frac{|T_{11}^{**} + T_{12}^{**} + T_{21}^{**} + T_{22}^{**}|}{2} \right) + 10 \log \left(\frac{S_1}{S_{12}} \right), \qquad (21)$$

$$OBJ_{22} = SWL_T(Q, RT_1^{***}, RT_2^{***}, RT_3^{***}, RT_4^{***}, RT_5^{***}, RT_6^{***}, RT_7^{***}, L_o, D_o). \qquad (22)$$

Likewise, the objective functions (OBJ_{31}, OBJ_{32}) in maximizing the STL at the pure tone (f) and minimizing the overall SWL for a one-chamber with a perforated plug-inlet tube are

$$OBJ_{31} = STL(Q, f, RT_1, RT_2, RT_3, RT_4, RT_5, RT_6, RT_7, L_o, D_o)$$
$$= 20 \log \left(\frac{|T_{11}^{***} + T_{12}^{***} + T_{21}^{***} + T_{22}^{***}|}{2} \right) + 10 \log \left(\frac{S_1}{S_7} \right), \qquad (23)$$

$$OBJ_{32} = SWL_T(Q, RT_1, RT_2, RT_3, RT_4, RT_5, RT_6, RT_7, L_o, D_o). \qquad (24)$$

Likewise, the objective functions (OBJ_{41}, OBJ_{42}) in maximizing the STL at the pure tone (f) and minimizing the overall SWL for a two-chamber muffler with perforated plug-inlet tubes are

$$OBJ_{41} = STL(Q, f, RT_1^*, RT_2^*, RT_3^*, RT_4^*, RT_5^*, RT_6^*, RT_7^*,$$
$$RT_8^*, RT_9^*, RT_{10}^*, RT_{11}^*, RT_{12}^*, RT_{13}^*, L_o, D_o)$$
$$= 20 \log \left(\frac{|T_{11}^{****} + T_{12}^{****} + T_{21}^{****} + T_{22}^{****}|}{2} \right) + 10 \log \left(\frac{S_1}{S_{12}} \right). \qquad (25)$$

The objective function in depressing the overall SWL is

$$OBJ_{42} = SWL(Q, RT_1^*, RT_2^*, RT_3^*, RT_4^*, RT_5^*, RT_6^*, RT_7^*,$$
$$RT_8^*, RT_9^*, RT_{10}^*, RT_{11}^*, RT_{12}^*, RT_{13}^*, L_o, D_o). \qquad (26)$$

3. Model check

Before performing the *SA* optimal simulation on mufflers, an accuracy check of the mathematical model on the one-chamber perforated plug muffler is performed using the experimental data from SULLIVAN *et al.* and MUNJAL [4, 5, 9]. As depicted in Fig. 14, accuracy between the theoretical and experiment data is in agreement.
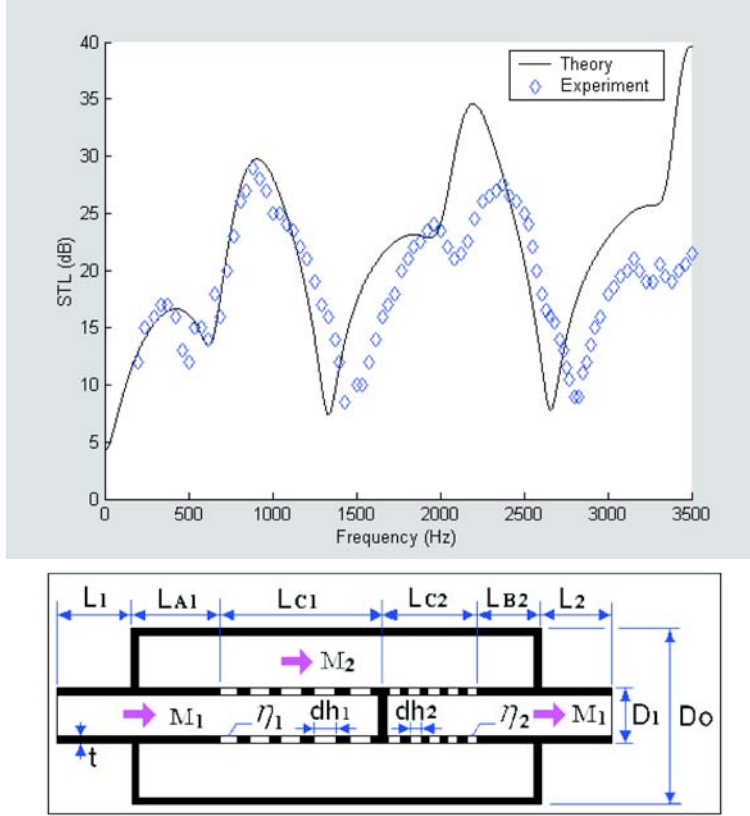

Fig. 14. Performance of a one-chamber perforated plug muffler with the mean flow [$M_1 = M_2 = 0.05$, $D_1 = 0.0493$ (m), $Do = 0.1016$ (m), $L_{C1} = L_{C2} = 0.1286$ (m), $L_1 = L_2 = 0.1$ (m), $L_{A1} = L_{B2} = 0.0$ (m), $t = 0.081$ (m), $dh_1 = dh_2 = 0.00249$ (m), $\eta_1 = \eta_2 = 0.037$]. [Experiment data is from SULLIVAN [3, 4]].

The proposed fundamental mathematical model is valid under the theoretical cutoff frequency of f_c which is given by

$$f_{C1} = \frac{1.84 c_o}{\pi D} (1 - M^2)^{1/2} = 1976 \text{ Hz}, \tag{27}$$

where D and M refer to the maximum diameter and Mach number of the muffler, respectively. Consequently, the model linked with the numerical method is applied for the shape optimization in the following section.

4. Case studies

In this paper, a blower confined within a R.C. (Reinforced Concrete) room is shown in Fig. 1. The noise level in the equipment venting outlet is remarkably high. To efficiently depress the noise, the multi-chamber muffler conjugated with either the perforated plug-inlet tubes or the extended inlet tubes is considered. The spectrum of exhausted sound power level (SWL) at the muffler inlet is shown in Table 1.

Table 1. The spectrum of exhausted sound power level (SWL).

f (Hz)	125	250	500	1k	2k	overall SWL
SWL (dB)	100	115	110	105	95	116.6

Before the minimization of broadband noise is performed, the maximization of the STL with respect to both a one-chamber and a two-chamber muffler conjugated with either a perforated plug-inlet tube or an extended inlet tube at targeted pure tones (800 Hz and 400 Hz) has been performed for the purpose of an accuracy check on the SA method. As shown in Fig. 1, the available space for a muffler is 0.6 m in width, 0.6 m in height and 1.5 m in length. To simplify the optimization, the flow rate ($Q = 0.01$ (m³/s)) and thickness of the perforated tube ($t = 0.0015$ (m)) are preset in advance. The corresponding space constraints and the ranges of design parameters for each muffler are summarized in Tables 2–3.

**Table 2.** Range of design parameters for multi-chamber muffler with plug-inlet tubes.

Muffler Type	Range of design parameters
One-chamber muffler with a perforated plug-inlet tube	Targeted $f = 800$ (Hz); $Q = 0.01$ (m³/s); $L_o = 1.5$ (m); $D_o = 0.6$ (m); RT_1:[0.2, 0.8]; RT_2:[0.2, 0.8]; RT_3:[0.1, 0.5]; RT_4:[0.1, 0.5]; RT_5:[0.2, 0.8]; RT_6:[0.03, 0.1]; RT_7:[0.00175, 0.007]
Two-chamber muffler with perforated plug-inlet tubes	Targeted $f = 400$ (Hz); $Q = 0.01$ (m³/s); $L_o = 1.5$ (m); $D_o = 0.6$ (m); RT_1^*:[0.2, 0.8]; RT_2^*:[0.2, 0.8]; RT_3^*:[0.2, 0.8]; RT_4^*:[0.2, 0.8]; RT_5^*:[0.00175, 0.007]; RT_6^*:[0.2, 0.8]; RT_7^*:[0.2, 0.8]; RT_8^*:[0.00175, 0.007]; RT_9^*:[0.1, 0.5]; RT_{10}^*:[0.1, 0.5]; RT_{11}^*:[0.1, 0.5]; RT_{12}^*:[0.03, 0.1]; RT_{13}^*:[0.03, 0.1]

Table 3. Range of design parameters for multi-chamber muffler with extended inlet tubes.

Muffler Type	Range of design parameters
One-chamber muffler with an extended inlet duct	Targeted $f = 800$ (Hz); $Q = 0.01$ (m^3/s); $L_o = 1.5$ (m); $D_o = 0.6$ (m); RT_1^{**}:[0.2, 0.8]; RT_2^{**}:[0.2, 0.8]; RT_3^{**}:[0.1, 0.5]; RT_4^{**}:[0.1, 0.5]
Two-chamber muffler with extended inlet ducts	Targeted $f = 400$ (Hz); $Q = 0.01$ (m^3/s); $L_o = 1.5$ (m); $D_o = 0.6$ (m); RT_1^{***}:[0.2, 0.8]; RT_2^{***}:[0.2, 0.8]; RT_3^{***}:[0.2, 0.8]; RT_4^{***}:[0.2, 0.8]; RT_5^{***}:[0.1, 0.5]; RT_6^{***}:[0.1, 0.5]; RT_7^{***}:[0.1, 0.5]

5. Simulated annealing method

The basic concept behind *SA* was first introduced by METROPOLIS *et al.* [12] and developed by KIRKPATRICK *et al.* [13]. *SA* simulates the annealing of metal. As indicated in Fig. 15, annealing is the process of heating and keeping the metal at a stabilized temperature while cooling it slowly. Slow cooling allows the particles to keep their state close to the minimal energy state. In this state, the particles have a more homogeneous crystalline structure. Conversely, a fast cooling rate results in a higher distortion energy stored inside the imperfect lattice. The purpose of the *SA* is to avoid stacking of local optimal solutions during optimization.
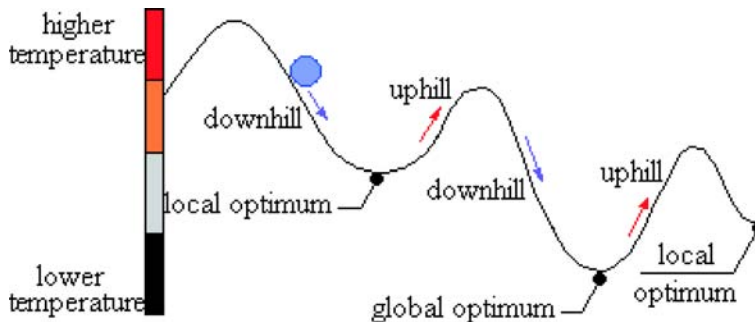
Fig. 15. *SA* method from a physical viewpoint.

The algorithm starts by generating a random initial solution. The scheme of the *SA* is a variation of the hill-climbing algorithm. All downhill movements for improvement are accepted for the decrement of the system's energy. Simultaneously, in order to escape from the local optimum, the *SA* also allows movement resulting in solutions that are worse (uphill moves) than the current solution. As

indicated in Fig. 16, to imitate the evolution of the *SA* algorithm, a new random solution (X') is chosen from the neighborhood of the current solution (X). If the change in objective function (or energy) is negative $(\Delta F \leq 0)$, the new solution will be acknowledged as the new current solution with the transition property (*pb(X') of 1*). If the change is not negative $(\Delta F > 0)$, the new transition property $(pb(X'))$ varied from 0–1 will be calculated first by the Boltzmann's factor $(pb(X') = \exp(\Delta F/CT))$ as shown in Eq. (28).
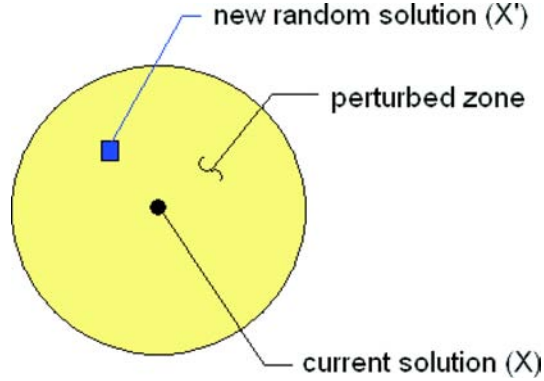
Fig. 16. New random solution in a perturbed zone.

$$pb(X') = \begin{cases} 1, & \Delta F \leq 0 \\ \exp\left(\dfrac{-\Delta F}{CT}\right), & \Delta F > 0 \end{cases} \tag{28}$$

$$\Delta F = F(X') - F(X),$$

wherein the C and T are the Boltzmann constant and the current temperature. If the transition property $(pb(X'))$ is greater than the random number of rand(0,1), the new solution (a worse solution) which results in a higher energy condition will then be accepted; otherwise, it is rejected. The algorithm repeats the perturbation of the current solution and the measurement of the change in the objective function. To reach an initial transition probability of 0.5, the initial temperature (T_o) is selected as 0.2 [16].

Each successful substitution of the new current solution will lead to the decay of the current temperature as

$$T_{\text{new}} = kk * T_{\text{old}},$$

where kk is the cooling rate. The process is repeated until the predetermined number (*Iter*) of the outer loop is reached.

The flow diagram of the *SA* optimization is described and shown in Fig. 17. As indicated, the *SA* optimization process with respect to objective functions $(OBJ_{11}, OBJ_{12}, OBJ_{21}, OBJ_{22}, OBJ_{31}, OBJ_{32}, OBJ_{41}, OBJ_{42})$ were performed by varying the control parameters – kk and *Iter*.
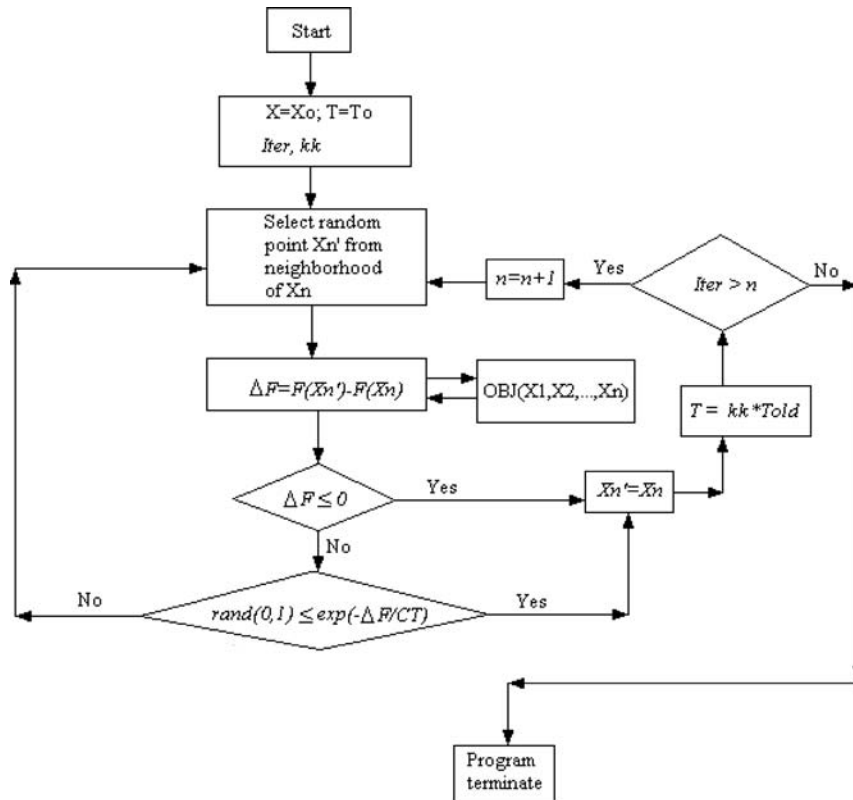
Fig. 17. Flow diagram of a SA optimization.

6. Results and discussion

6.1. Results

The accuracy of the SA optimization depends on the cooling rate (kk) and the number of iterations ($Iter$). To investigate the influences of the cooling rate and the number of iterations, the assessed ranges of the SA parameters of the cooling rate and the iterations are

$$kk = (0.90, 0.93, 0.96, 0.99); \quad Iter = (25, 50, 100, 200).$$

The results of two kinds of optimizations, one of the pure tone noise and the others of the broadband noise, are described as follows:

A. Pure Tone Noise Optimization

By using Eqs. (23) and (25), the maximization of the STL with respect to two kinds of mufflers (one-chamber and two chamber mufflers hybridized with perforated plug-inlet tubes) at the pure tones (400 Hz and 800 Hz) was performed. As indicated in Tables 4 and 5, seven sets of SA parameters are tried in the muffler's optimization.

Table 4. Optimal design data for a one-chamber muffler with a plug-inlet tube (targeted tone at 800 Hz).

SA parameter		Design parameters							Performance
$Iter$	kk	RT_1	RT_2	RT_3	RT_4	RT_5	RT_6	RT_7	STL (dB)
25	0.90	0.3202	0.3202	0.1801	0.1801	0.3202	0.04402	0.0028	45.0
25	0.93	0.2614	0.2614	0.1409	0.1409	0.2614	0.03716	0.00229	52.0
25	0.96	0.2406	0.2406	0.1271	0.1271	0.2406	0.03474	0.00211	56.7
25	0.99	0.2590	0.2590	0.1393	0.1393	0.2590	0.03688	0.00227	52.5
50	0.96	0.3624	0.3624	0.2082	0.2082	0.3624	0.04894	0.00317	58.0
100	0.96	0.2252	0.2252	0.1168	0.1168	0.2252	0.03294	0.00197	60.9
200	**0.96**	**0.3594**	**0.3594**	**0.2063**	**0.2063**	**0.3594**	**0.04860**	**0.00315**	**63.9**

Table 5. Optimal design data for a two-chamber muffler with plug-inlet tubes (targeted tone at 400 Hz).

| SA parameter		Design parameters													Performance
$Iter$	kk	RT_1^*	RT_2^*	RT_3^*	RT_4^*	RT_5^*	RT_6^*	RT_7^*	RT_8^*	RT_9^*	RT_{10}^*	RT_{11}^*	RT_{12}^*	RT_{13}^*	SWL (dB)
25	0.90	0.27	0.27	0.27	0.27	0.00236	0.27	0.27	0.00236	0.1467	0.1467	0.1467	0.0382	0.0382	82.9
25	0.93	0.261	0.261	0.261	0.261	0.00229	0.261	0.261	0.00229	0.1409	0.1409	0.1409	0.0372	0.0372	88.5
25	0.96	0.237	0.237	0.237	0.237	0.00207	0.237	0.237	0.00207	0.1246	0.1246	0.1246	0.0343	0.0343	105.1
25	0.99	0.241	0.241	0.241	0.241	0.00211	0.241	0.241	0.00211	0.1271	0.1271	0.1271	0.0347	0.0347	102.5
50	0.96	0.230	0.230	0.230	0.230	0.00202	0.23	0.23	0.00202	0.1202	0.1202	0.1202	0.0335	0.0335	109.8
100	0.96	0.225	0.225	0.225	0.225	0.00197	0.225	0.225	0.00197	0.1168	0.1168	0.1168	0.0329	0.0329	113.5
200	**0.96**	**0.219**	**0.219**	**0.219**	**0.219**	**0.00191**	**0.219**	**0.219**	**0.00191**	**0.1125**	**0.1125**	**0.1125**	**0.0329**	**0.0329**	**118.4**
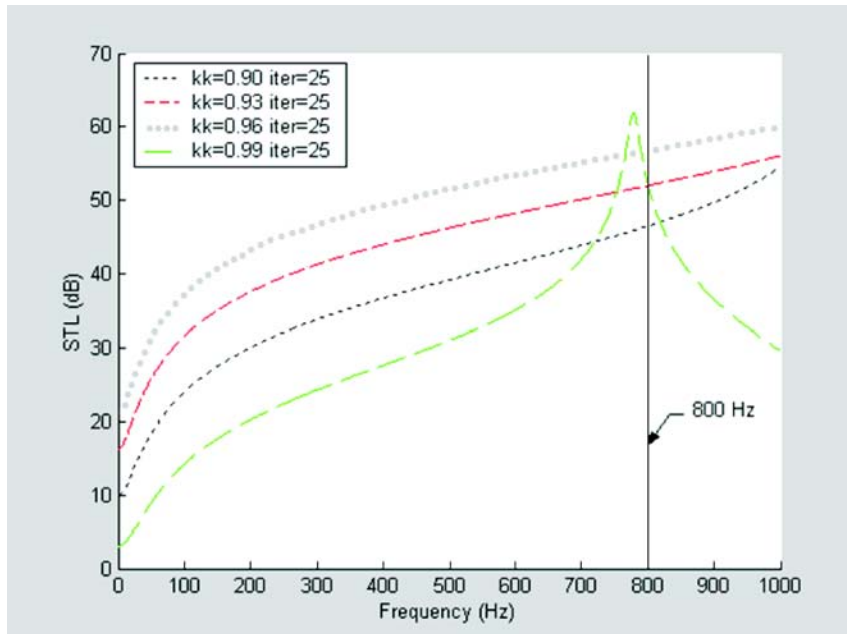
Fig. 18. Optimal *STL* with respect to various cooling rates (*kk*) for a one-chamber muffler hybridized with a perforated plug-inlet tube (targeted tone: 800 Hz).
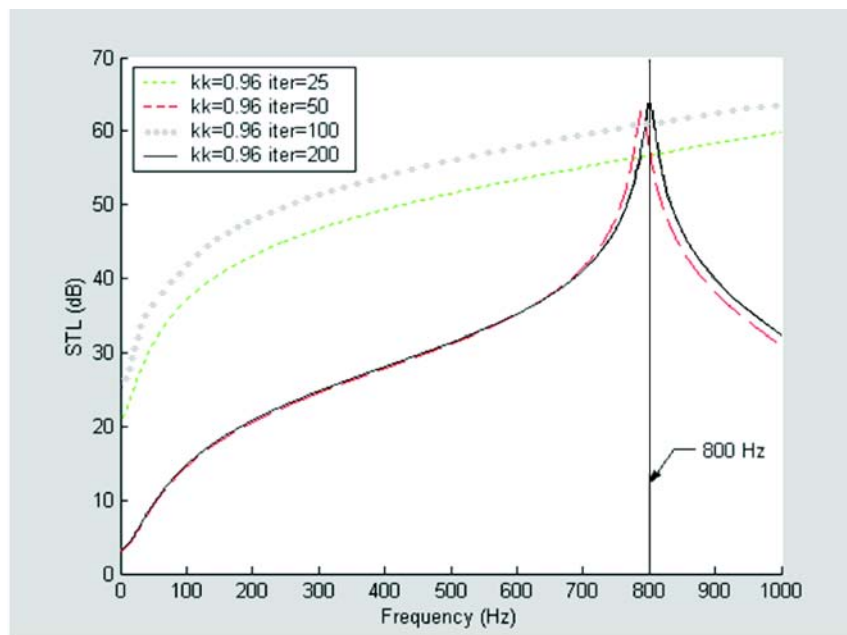

Fig. 19. Optimal *STL* with respect to various iteration (*Iter*) for a one-chamber muffler hybridized with a perforated plug-inlet tube (targeted tone: 800 Hz).
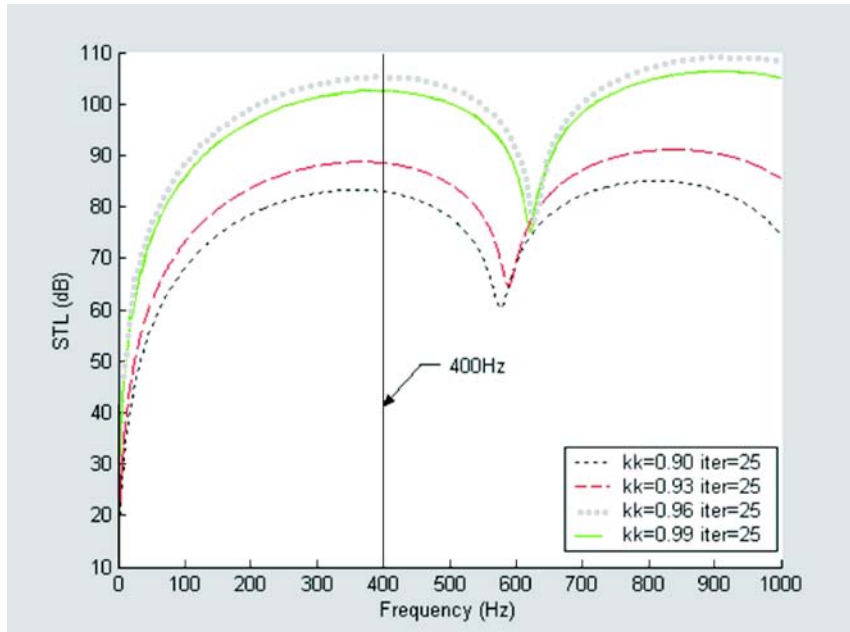
Fig. 20. Optimal *STL* with respect to various cooling rates (*kk*) for a two-chamber muffler hybridized with perforated plug-inlet tubes (targeted tone: 400 Hz).
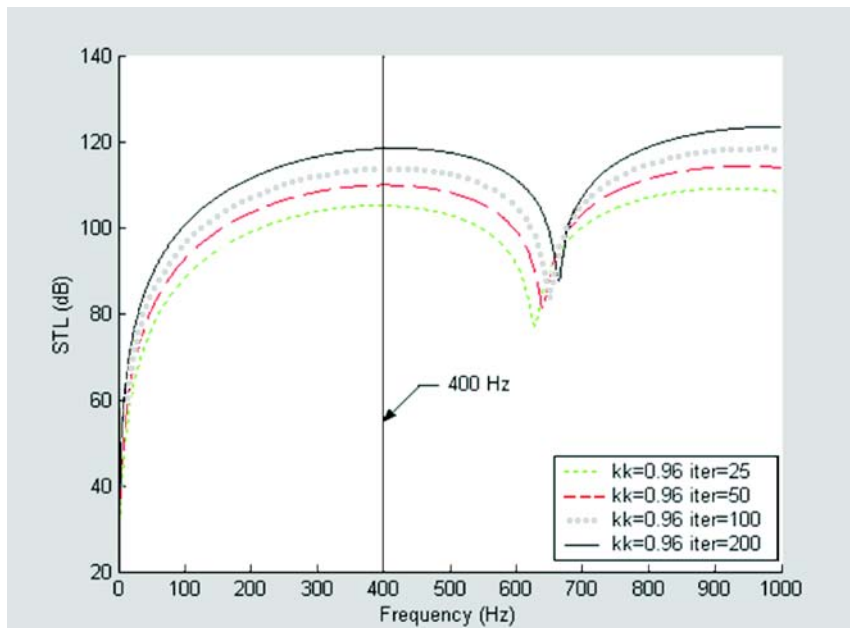

Fig. 21. Optimal *STL* with respect to various iteration (*Iter*) for a two-chamber muffler hybridized with perforated plug-inlet tubes (targeted tone: 400 Hz).
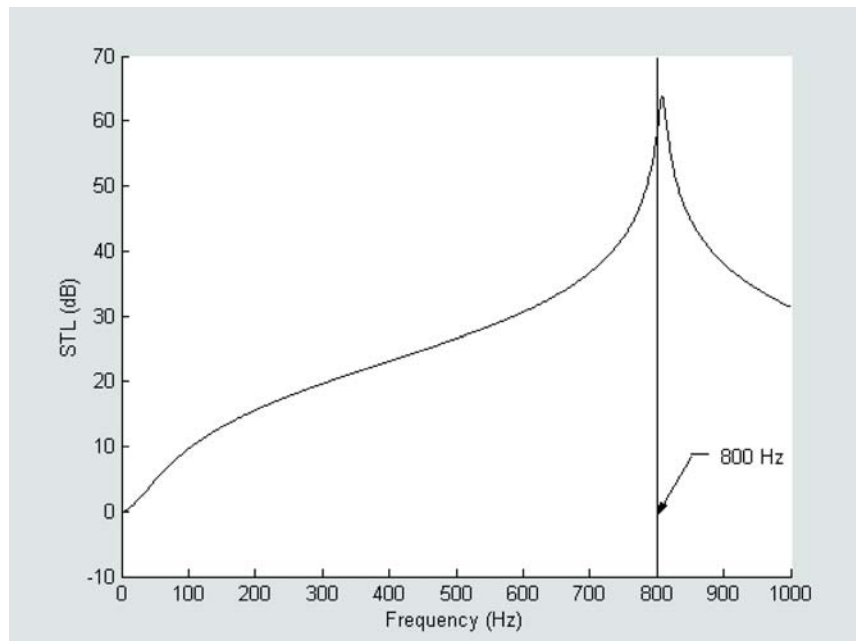
Fig. 22. Optimal *STL* for a one-chamber muffler hybridized with an extended inlet tube at a desired tone of 800 Hz.
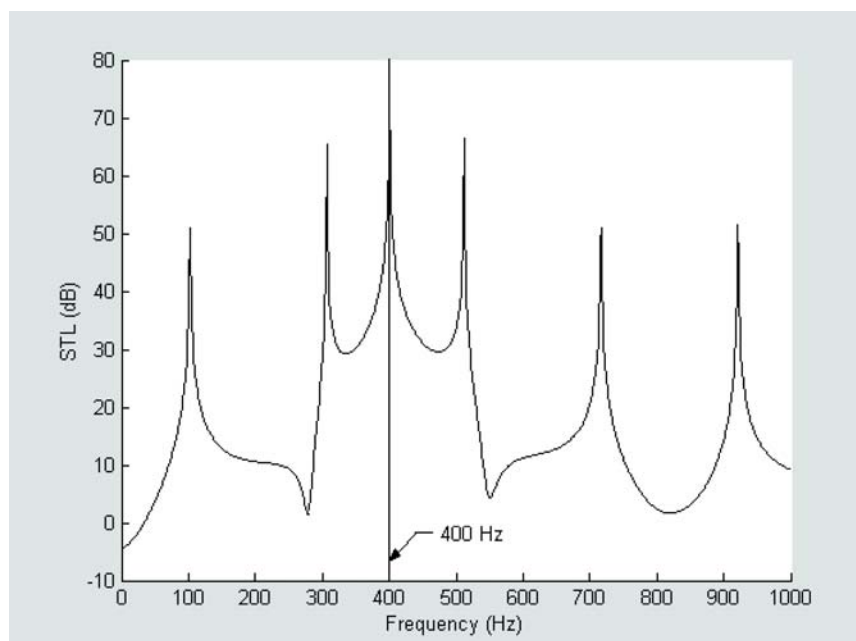

Fig. 23. Optimal *STL* for a two-chamber muffler hybridized with extended inlet tubes at a desired tone of 400 Hz.

Obviously, the optimal design data can be obtained from the last set of *SA* parameters at (*kk, Iter*) = (0.96, 200). Using the optimal design data in a theoretical calculation, the resultant curves of the *STL* with respect to various *SA* parameters (*kk, Iter*) for a one-chamber muffler hybridized with a perforated plug-inlet tube at a targeted tone (400 Hz) are depicted in Figs. 18 and 19.

Likewise, the resultant curves with respect to various *SA* parameters (*kk, Iter*) for a two-chamber muffler hybridized with perforated plug-inlet tubes at a targeted tone (400 Hz) are depicted in Figs. 20 and 21. As revealed in Figs. 19 and 21, the *STL*s are precisely maximized at the desired frequencies of 400 Hz and 800 Hz when the *SA* parameters set is at (*kk, Iter*) = (0.96, 200).

In order to distinguish the acoustical influence of a perforated and plugged tube, the shape optimization of the multi-chamber mufflers hybridized with extended inlet tubes at pure tones (400 Hz and 800), using Eqs. (19), (21) in conjunction with the *SA* set of (*kk, Iter*) = (0.96, 200), is performed. The resultant *STL* curves for two kinds of mufflers (one-chamber and two-chamber mufflers hybridized with extended inlet tubes) at targeted tones are depicted in Tables 6–7 and Figs. 22–23. As revealed in Figs. 22 and 23, the *STL*s are also precisely maximized at the desired frequencies of 400 Hz and 800 Hz.

Table 6. Optimal design data for a one-chamber muffler with an extended inlet tube (targeted tone at 800 Hz).

SA parameter		Design parameters				Performance
Iter	*kk*	RT_1^{**}	RT_2^{**}	RT_3^{**}	RT_4^{**}	*STL* (dB)
200	0.96	0.3244	0.3244	0.1830	0.1830	58.1

Table 7. Optimal design data for a two-chamber muffler with extended inlet tubes (targeted tone at 400 Hz).

SA parameter		Design parameters							Performance
Iter	*kk*	RT_1^{***}	RT_2^{***}	RT_3^{***}	RT_4^{***}	RT_5^{***}	RT_6^{***}	RT_7^{***}	*STL* (dB)
200	0.96	0.7442	0.7442	0.7442	0.7442	0.4628	0.4628	0.4628	71.1

B. Broadband Noise Optimization

By using the formulas of Eqs. (20), (22), (24), (26) and the *SA* parameters of (*kk* = 0.96, *Iter* = 200), four kinds of optimal design parameters for minimizing the sound power level at the muffler's outlet are obtained and summarized in Table 8.

As illustrated in Table 8, the resultant sound power level of the one-chamber muffler with an extended inlet tube has been reduced from 116.6 dB to 96.5 dB. In addition, the resultant sound power level of the two-chamber muffler with two extended inlet tubes has been reduced to 84.1 dB. Similarly, the reduced sound power level of the one-chamber muffler with a perforated plug-inlet tube
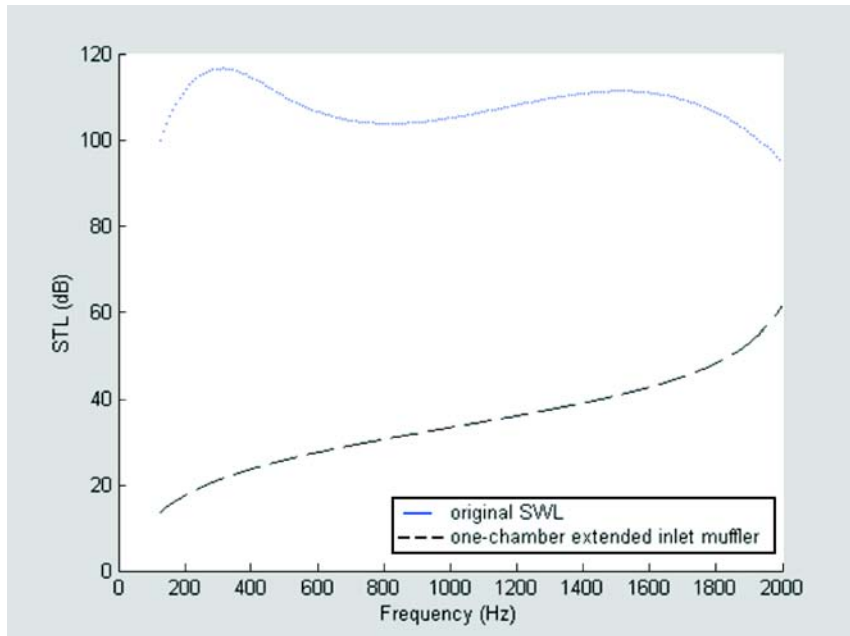
Table 8. Optimal design data and overall SWL for four kinds of mufflers ($kk = 0.96$, $Iter = 200$) (broadband).

Item No.	Design parameters													SWL_T (dB)
#1	RT_1^{**} 0.2044	RT_2^{**} 0.2044	RT_3^{**} 0.1030	RT_4^{**} 0.1030										96.5
#2	RT_1^{***} 0.2168	RT_2^{***} 0.2168	RT_3^{***} 0.2168	RT_4^{***} 0.2168	RT_5^{***} 0.1112	RT_6^{***} 0.1112	RT_7^{***} 0.1112							84.1
#3	RT_1 0.2168	RT_2 0.2168	RT_3 0.1112	RT_4 0.1112	RT_5 0.2168	RT_6 0.0320	RT_7 0.0019							63.6
#4	RT_1^{*} 0.219	RT_2^{*} 0.219	RT_3^{*} 0.219	RT_4^{*} 0.219	RT_5^{*} 0.00191	RT_6^{*} 0.219	RT_7^{*} 0.219	RT_8^{*} 0.00191	RT_9^{*} 0.1125	RT_{10}^{*} 0.1125	RT_{11}^{*} 0.1125	RT_{12}^{*} 0.0322	RT_{13}^{*} 0.0322	9.8

Note:
#1 is a one-chamber muffler with an extended inlet tube;
#2 is a two-chamber muffler with extended inlet tubes;
#3 is a one-chamber muffler with a perforated plug-inlet tube;
#4 is a two-chamber muffler with perforated plug-inlet tubes.

Fig. 24. Optimal *STL* for a one-chamber muffler hybridized with an extended inlet tube (broadband noise).
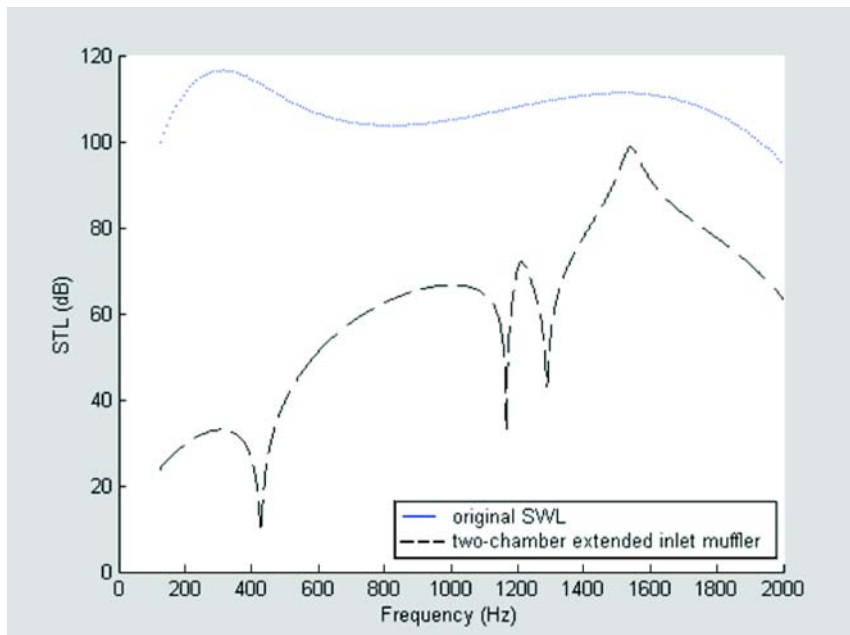

Fig. 25. Optimal *STL* for a two-chamber muffler hybridized with extended inlet tubes (broadband noise).
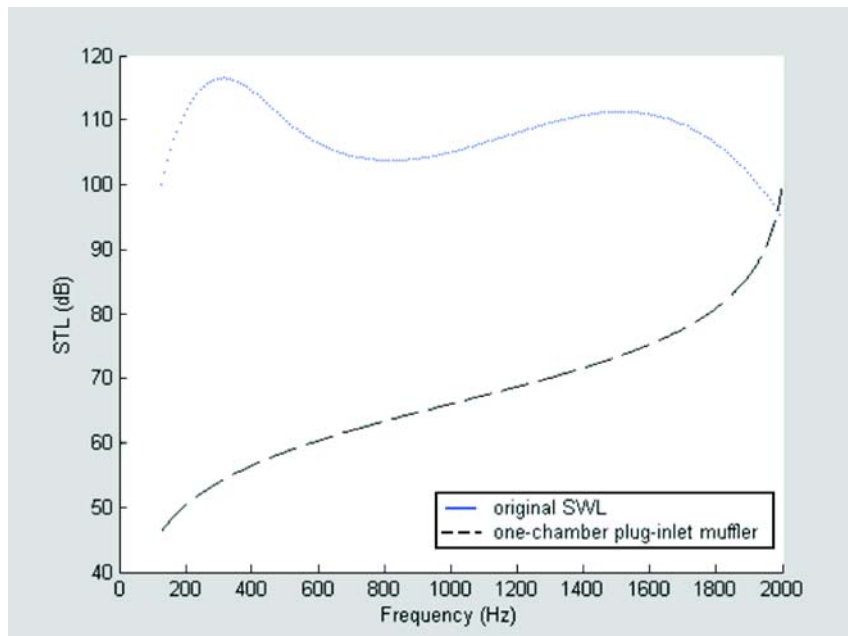
Fig. 26. Optimal *STL* for a one-chamber muffler hybridized with a perforated plug-inlet tube (broadband noise).
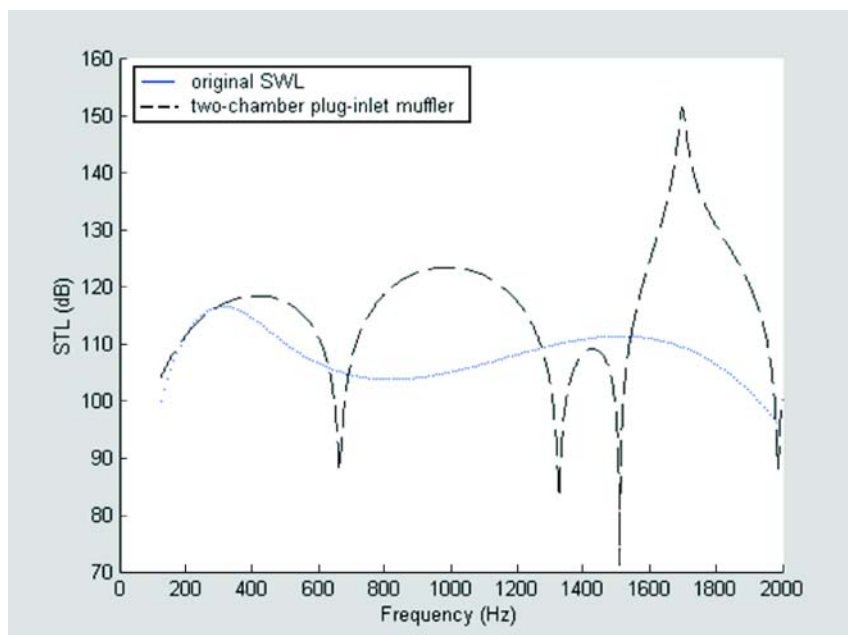

Fig. 27. Optimal *STL* for a two-chamber muffler hybridized with perforated plug-inlet tubes (broadband noise).

is 63.6 dB. The reduced sound power level of the two-chamber muffler with two perforated plug-inlet tubes is 9.8 dB. The resultant curves of the *STL* with respect to various mufflers are depicted in Figs. 24–27.

6.2. Discussion

To achieve a better optimization, the selection of the appropriate set of *SA* parameters is essential. As indicated in Tables 4 and 5, the seventh *SA* set has a better solution during the shape optimization of multi-chamber and perforated plug-inlet mufflers at the pure tones. In order to evaluate the acoustical efficiency, the optimization of multi-chamber mufflers hybridized with extended inlet tubes under the same space-limited condition are investigated and compared to each other in Figs. 28–29.

As indicated in Figs. 28–29, the predicted maximal values of the *STL*s are precisely located at the desired frequencies. Moreover, it is obvious that the muffler with the perforated plug-inlet has a better acoustical performance by a margin of 5.8–47.3 dB than the muffler with an extended inlet tube.

Moreover, in dealing with the broadband noise, a comparison of the acoustical performance between the four kinds of mufflers is depicted in Fig. 30.

As indicated in Fig. 30, the two-chamber muffler with perforated plug-inlet tubes has the best acoustical performance. Furthermore, the acoustical performance of the one-chamber muffler with a perforated plug-inlet tube is superior
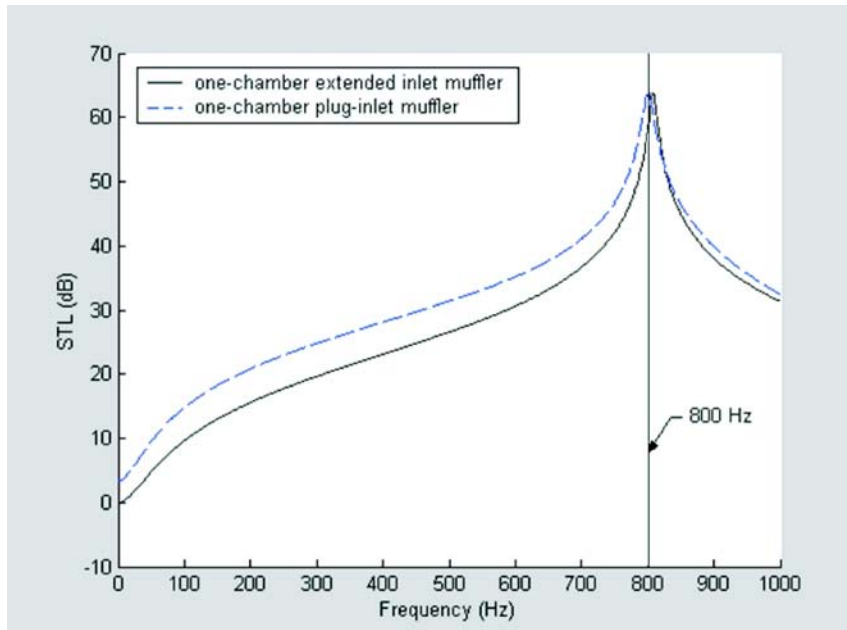

Fig. 28. A comparison of a one-chamber muffler hybridized with a perforated plug-inlet and an extended plug inlet tube(targeted tone: 800 Hz).
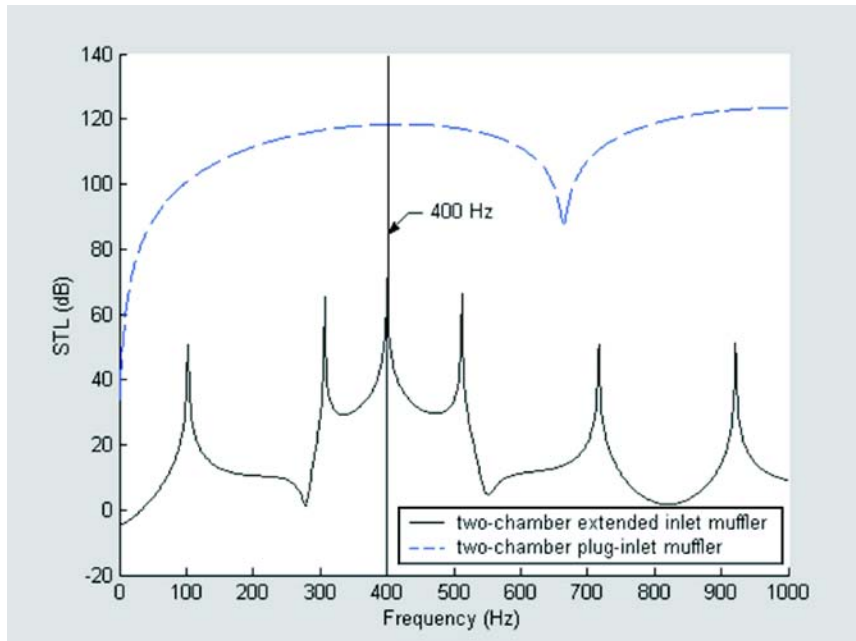
Fig. 29. A comparison of a two-chamber muffler hybridized with perforated plug-inlet and extended inlet tubes(targeted tone: 400 Hz).
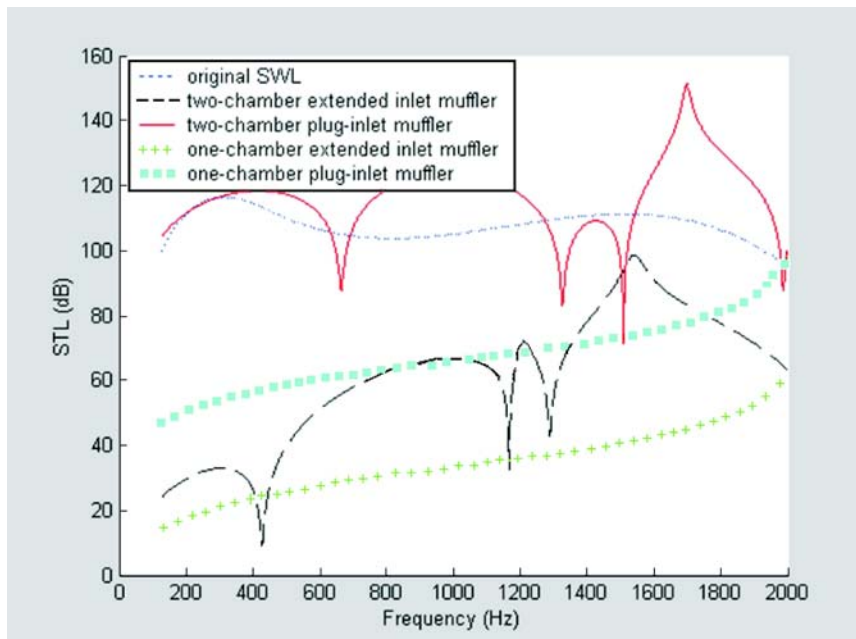

Fig. 30. A comparison of four kinds of mufflers (broadband noise).

to that of the one-chamber and two-chamber mufflers with extended inlet tubes. Likewise, the one-chamber muffler with an extended inlet tube has the worst acoustical performance.

As indicated in Table 8, the noise reductions with respect to the four kinds of mufflers (two-chamber muffler with two perforated plug-inlet, one-chamber muffler with a perforated plug-inlet, two-chamber muffler with extended inlet tubes, and one-chamber muffler with an extended inlet tube) are 106.8 dB, 53 dB, 32.5 dB, and 20.1 dB. Obviously, the muffler with the acoustical mechanism of a perforated plug-inlet is superior to that of the extended inlet tube. Moreover, the muffler with more chambers will also result in a better in noise reduction.

7. Conclusion

To achieve an optimal muffler shape under the space constraints, the *SA* optimizer conjugated with a generalized decoupling technique, a plane wave theory, as well as a four-pole transfer matrix method, is utilized and found to be easy and efficient. It has been shown that two kinds of *SA* parameters – *kk* and *Iter* – play essential roles in the solution's accuracy during the *SA* optimization. Results reveal that the predicted maximal values of the *STL*'s acoustical performance are precisely located at the desired frequencies. In addition, the appropriate acoustical performance curve of the muffler in depressing overall broadband noise has been assessed. As indicated in Table 8, when using a two-chamber muffler with two perforated plug-inlet tubes, the resultant noise energy level can be dramatically reduced from 116.6 dB to 9.8 dB(A).

As indicated in Fig. 30, the *STL* curves with respect to various mufflers are plotted. It is clear that these multi-chamber mufflers which are hybridized with perforated plug-inlet tubes, are superior to those mufflers which are conjugated with extended inlet tubes. Moreover, the more chambers a muffler has, the higher acoustical performance it will have.

Consequently, the approach used for the optimal design of the *STL* proposed in this study is indeed easy and quite effective.

Appendix A. Transfer matrix of a straight duct

For a three-dimensional wave within a moving medium, the resultant wave governing equation is [14]

$$\left(\frac{\partial^2}{\partial t^2} - c_o^2 \nabla^2 \right) p = 0, \tag{29}$$

where the Laplacian ∇^2 with respect to the cylindrical system shown in Fig. 31 is

$$\nabla^2 = \frac{\partial^2}{\partial r^2} + \frac{1}{r} \frac{\partial}{\partial r} + \frac{1}{r^2} \frac{\partial^2}{\partial \theta^2} + \frac{\partial^2}{\partial z^2}. \tag{30}$$
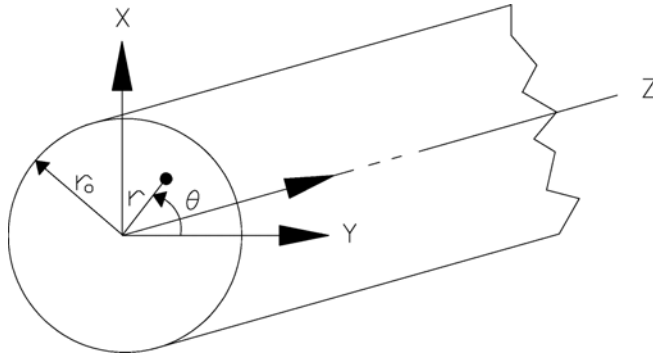
Fig. 31. Cylindrical polar coordinate system of a straight duct.

By using the separation of variables method in Eqs. (29) and (30), it yields [14]

$$p(r,\theta,z,t) = \sum_{m=0}^{\infty} \sum_{n=0}^{\infty} J_m(k_{r,m,n}r)\left(C_{1,m,n}e^{-jk_{z,m,n}^+z} + C_{2,m,n}e^{+jk_{z,m,n}^-z}\right)e^{j\omega t}, \quad (31)$$

$$u_z(r,\theta,z,t)$$

$$= \frac{1}{\rho_o c_o}\sum_{m=0}^{\infty}\sum_{n=0}^{\infty} J_m(k_{r,m,n}r)e^{jm\theta}e^{j\omega t}\left(\begin{array}{c}\dfrac{k_{z,m,n}^+}{k_o - Mk_{z,m,n}^+}C_{1,m,n}e^{-jk_{z,m,n}^+z}\\[2mm] +\dfrac{k_{z,m,n}^-}{k_o + Mk_{z,m,n}^+}C_{2,m,n}e^{+jk_{z,m,n}^-z}\end{array}\right), \quad (32)$$

$$k_{z,m,n}^{\pm} = \frac{\mp Mk_o + \left[k_o^2 - (1-M^2)k_{r,m,n}^2\right]^{1/2}}{1 - M^2}. \quad (33)$$

For the fundamental mode of ($m = 0$, $n = 0$), only a plane wave would propagate if the frequencies of f were smaller than the cut-off frequency of f_c where

$$f_{c1} = \frac{1.84c_o}{\pi D}(1 - M^2)^{1/2}. \quad (34)$$

For a one-dimensional wave propagating in a symmetric straight duct shown in Fig. 32, the acoustic pressure and particle velocity are reduced to

$$p(x,t) = \left(c_1 e^{-jkx/(1+M)} + c_2 e^{+jkx/(1-M)}\right)e^{j\omega t}, \quad (35)$$

$$u(x,t) = \left(\frac{c_1}{\rho_o c_o}e^{-jkx/(1+M)} - \frac{c_2}{\rho_o c_o}e^{+jkx/(1-M)}\right)e^{j\omega t}. \quad (36)$$

Considering boundary conditions of pt 1 ($x = 0$) and pt 2 ($x = L$), Eqs. (35) and (36) can be rearranged as

$$\begin{pmatrix} p_1 \\ \rho_o c_o u_1 \end{pmatrix} = \begin{bmatrix} 1 & 1 \\ 1 & -1 \end{bmatrix}\begin{pmatrix} c_1 \\ c_2 \end{pmatrix}, \quad (37)$$
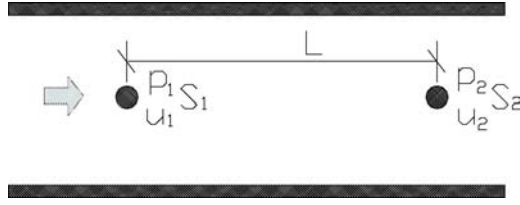
Fig. 32. Sound propagation inside a straight duct.

$$\begin{pmatrix} p_2 \\ \rho_o c_o u_2 \end{pmatrix} = \begin{bmatrix} e^{-jk^+L} & e^{+jk^-L} \\ e^{-jk^+L} & -e^{+jk^-L} \end{bmatrix} \begin{pmatrix} c_1 \\ c_2 \end{pmatrix}, \tag{38$_1$}$$

where

$$k^+ = \frac{k}{1+M_1}, k^- = \frac{k}{1-M_1}. \tag{38$_2$}$$

Combination of Eqs. (37) and (38) becomes

$$\begin{pmatrix} p_1 \\ \rho_o c_o u_1 \end{pmatrix} = e^{-j\frac{M_1 kL}{1-M_1^2}} \begin{bmatrix} \cos\left(\frac{kL}{1-M_1^2}\right) & j\sin\left(\frac{kL}{1-M_1^2}\right) \\ j\sin\left(\frac{kL}{1-M_1^2}\right) & \cos\left(\frac{kL)}{1-M_1^2}\right) \end{bmatrix} \begin{pmatrix} p_2 \\ \rho_o c_o u_2 \end{pmatrix}$$

$$= e^{-j\frac{M_1 kL}{1-M_1^2}} \begin{bmatrix} TS_{1,1} & TS_{1,2} \\ TS_{2,1} & TS_{2,2} \end{bmatrix} \begin{pmatrix} p_2 \\ \rho_o c_o u_2 \end{pmatrix}, \tag{39$_1$}$$

where

$$TS1_{1,1} = \cos\left[\frac{kL}{1-M_1^2}\right], \qquad TS1_{1,2} = j\sin\left[\frac{kL}{1-M^2}\right],$$

$$TS1_{2,1} = j\sin\left[\frac{kL}{1-M^2}\right], \qquad TS1_{2,2} = \cos\left[\frac{kL}{1-M^2}\right]. \tag{39$_2$}$$

Appendix B. Transfer matrix of an expanded extended duct

As indicated in Fig. 33, the equation of the mass continuity between point 2 and point 4 with a mean flow is expressed in Eq. (40).

$$c_o\rho_o S_2 u_2 + S_2 M_2 p_2 = c_o\rho_o S_4 u_4 + c_o\rho_o S_3 u_3$$
$$+ S_4 M_4 \left(p_4 - \frac{p_o}{C_v} \frac{RK_e M_4 Y_4}{p_o} \frac{v_{c,4} - M_4 p_{c,4}/Y_4}{1-M_4^2} \right), \tag{40$_1$}$$

or

$$c_o\rho_o S_2 u_2 + S_2 M_2 p_2 = c_o\rho_o S_4 u_4 + c_o\rho_o S_3 u_3$$
$$+ S_4 M_4 \left(p_4 - \frac{p_o(\gamma-1)K_e M_4 Y_4}{p_o} \frac{v_{c,4} - M_4 p_{c,4}/Y_4}{1-M_4^2} \right), \tag{40$_2$}$$

where

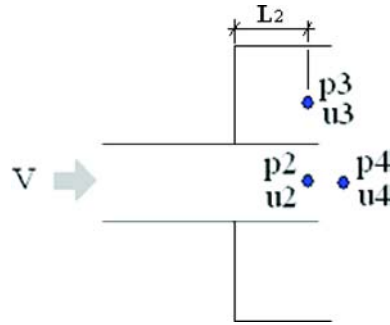$$K_e = \left[\frac{S_4}{S_2} - 1\right]^2. \tag{40}_3$$

Fig. 33. Acoustic field of an extended tube at inlet.

A concept of static enthalpy deduced by MUNJAL [14, 17] is described as

$$\begin{bmatrix} p_{c,4} \\ v_{c,4} \end{bmatrix} = \begin{bmatrix} 1 & M_4 Y_4 \\ M_4/Y_4 & 1 \end{bmatrix} \begin{bmatrix} p_4 \\ \rho_o S_4 u_4 \end{bmatrix}. \tag{41}$$

Combining Eq. (41) with Eq. (40), one has

$$c_o \rho_o S_2 u_2 + S_2 M_2 p_2$$
$$= c_o \rho_o S_4 u_4 \left[1 - \frac{(\gamma-1)}{c_o} Y_4 K_c S_4 M_4^2\right] + (M_4 S_4 p_4 + c_o \rho_o u_3 S_3). \tag{42}$$

The equation of momentum for a steady flow is

$$S_2 p_2 + 2\rho_o S_2 V_2 u_2 + S_2 M_2^2 p_2$$
$$= -c_{21} \begin{pmatrix} S_4 p_4 + 2\rho_o S_4 u_4 + \\ S_4 M_4^2 \left[p_4 - (\gamma-1)k_e M_4 Y_4 \dfrac{v_{c,4} - M_4 p_{c,4}/Y_4}{1 - M_4^2} \right] \end{pmatrix} - c_{22} S_3 p_3, \tag{43}_1$$

where

$$c_{21} = -1, \qquad c_{22} = 1. \tag{43}_2$$

Combining Eq. (41) with Eq. (43), we have

$$S_2 \left(1 + M_2^2\right) p_2 + 2\rho_o c_o S_2 M_2 u_2 + c_{21} \left(S_4 + S_4 M_4^2\right) p_4$$
$$= -c_{21} \left(\frac{2S_4}{c_o} - \frac{(\gamma-1)K_e M_4^3 Y_4 S_4^2}{c_o}\right) \rho_o c_o u_4 - c_{22} S_3 p_3. \tag{44}$$

The equation of energy conservation for a steady flow is

$$p_2 + \rho_o V_2 u_2 = p_4 + \rho_o V_4 u_4 + K_e \rho_o V_4 u_4. \tag{45}$$

With a rigid wall at the boundary, one has

$$\frac{p_3}{\rho_o c_o u_3} = -j\cot(kL_2),\tag{46}$$

By combining Eq. (46) with Eqs. (42), (44), and (45), the transfer matrix between pt2 and pt4 is thus illustrated by

$$\begin{pmatrix} p_2 \\ \rho_o c_o u_2 \end{pmatrix} = \begin{bmatrix} TSEE_{1,1} & TSEE_{1,2} \\ TSEE_{2,1} & TSEE_{2,2} \end{bmatrix} \begin{pmatrix} p_4 \\ \rho_o c_o u_4 \end{pmatrix}.\tag{47}$$

Appendix C. Transfer matrix of an expanded and perforated plug-inlet duct

As indicated in Fig. 34, the expansion perforated duct is composed of an inner perforated tube and an outer one-end opened duct. Based on SULLIVAN'S and CROCKER'S derivation [2], the continuity equations and momentum equations with respect to the inner and outer tubes at nodes 2 and 2A are as follows:
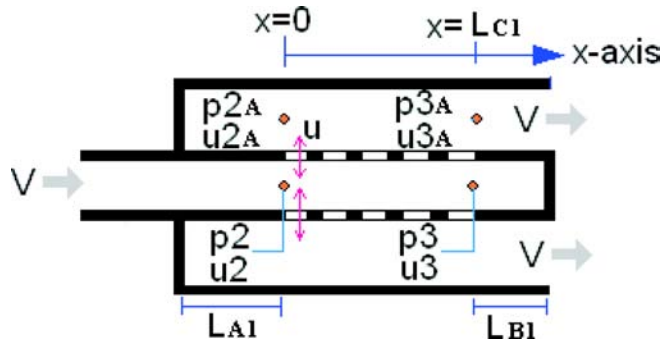

Fig. 34. Mechanism of an expanded and perforated plug-inlet tube.

Inner tube:
   • continuity equation

$$V\frac{\partial \rho_2}{\partial x} + \rho_o\frac{\partial u_2}{\partial x} + \frac{4\rho_o}{D_1}u + \frac{\partial \rho_{2A}}{\partial t} = 0,\tag{48}$$

   • momentum equation

$$\rho_o\left(\frac{\partial}{\partial t} + V\frac{\partial}{\partial x}\right)u_2 + \frac{\partial p_2}{\partial x} = 0.\tag{49}$$

Outer tube:
   • continuity equations

$$\rho_o\frac{\partial u_{2A}}{\partial x} - \frac{4D_1\rho_o}{D_o^2 - D_1^2}u + \frac{\partial \rho_{2A}}{\partial t} = 0,\tag{50}$$

$$\rho_o\frac{\partial u_{2A}}{\partial t} + \frac{\partial p_{2A}}{\partial x} = 0.\tag{51}$$

Assuming that the acoustic wave is a harmonic motion under the isentropic processes in ducts, we have

$$p(x,t) = \rho(x) \cdot c_o^2 \cdot e^{j\omega t}. \tag{52}$$

The acoustic impedance of the perforation $(c_o\xi)$ is expressed as

$$c_o\xi = \frac{p_2(x) - p_{2A}(x)}{u(x)}. \tag{53}$$

For perforations with stationary medium [7], we have

$$\xi = [0.006 + jk(t + 0.75dh)]/\eta. \tag{54}_1$$

For perforations with grazing flow [8], we have

$$\xi = [0.514D_1M/(L_{C1}\eta) + j0.95k(t + 0.75dh)]/\eta, \tag{54}_2$$

where dh is the diameter of a perforated hole on the inner tube, t is the thickness of the inner perforated tube, and η is the porosity of the perforated tube.

By combining Eqs. (52)–(53) with Eqs. (48)–(51) and eliminating u_2 and u_{2A}, we have

$$\left[\left(1 - M_2^2\right)\frac{d^2}{dx^2} - 2jM_2k\frac{d}{dx} + k^2\right]p_2 - \frac{4}{D_1\xi}\left[M_2\frac{d}{dx} + jk\right](p_2 - p_{2A}) = 0,$$

$$\left[\frac{d^2}{dx^2} + k^2\right]p_{2A} + j\frac{4D_1}{(D_o^2 - D_1^2)\xi}(p_2 - p_{2A}) = 0. \tag{55}$$

Alternatively, Eqs. $(55)_1$ and $(55)_2$ can also be expressed as [9]

$$p_2'' + \alpha_1 p_2' + \alpha_2 p_2 + \alpha_3 p_{2A}' + \alpha_4 p_{2A} = 0,$$

$$\alpha_5 p_2' + \alpha_6 p_2 + p_{2A}'' + \alpha_7 p_{2A}' + \alpha_8 p_{2A} = 0. \tag{56}$$

Let

$$p_2' = \frac{dp_2}{dx} = y_1, \qquad p_{2A}' = \frac{dp_{2A}}{dx} = y_2,$$

$$p_2 = y_3, \qquad\qquad p_{2A} = y_4. \tag{57}$$

According to Eqs. (56) and (57), the new matrix between $\{y'\}$ and $\{y\}$ is

$$\begin{bmatrix} y_1' \\ y_2' \\ y_3' \\ y_4' \end{bmatrix} = \begin{bmatrix} -\alpha_1 & -\alpha_3 & -\alpha_2 & -\alpha_4 \\ -\alpha_5 & -\alpha_7 & -\alpha_6 & -\alpha_8 \\ 1 & 0 & 0 & 0 \\ 0 & 1 & 0 & 0 \end{bmatrix} \begin{bmatrix} y_1 \\ y_2 \\ y_3 \\ y_4 \end{bmatrix}, \tag{58}_1$$

or

$$\{y'\} = [\Psi]\{y\}. \tag{58}_2$$

Let

$$\{y\} = [\Omega]\{\Gamma\}. \tag{59}$$

Combining Eq. (59) with (58) and then multiplying $[\Omega]^{-1}$ by both sides, it becomes

$$\{\Gamma'\} = [\chi]\{\Gamma\}, \tag{60}_1$$

where

$$[\chi] = [\Omega]^{-1}[\Psi][\Omega] = \begin{bmatrix} \lambda_1 & 0 & 0 & 0 \\ 0 & \lambda_2 & 0 & 0 \\ 0 & 0 & \lambda_3 & 0 \\ 0 & 0 & 0 & \lambda_4 \end{bmatrix}, \tag{60}_2$$

λ_i – the eigen-value of $[\Psi]$; $[\Omega]_{4\times4}$ – the model matrix formed by four sets of eigen-vectors $\Omega_{4\times1}$ of $[\Psi]_{4\times4}$.

The related solution of Eq. (60) then becomes

$$\Gamma_i = f_i e^{\lambda_i x}. \tag{61}$$

Using Eqs. (49), (51), (60) and (61), the relationship of the acoustic pressure and particle velocity yields

$$\begin{bmatrix} p_2(x) \\ p_{2A}(x) \\ \rho_o c_o u_2(x) \\ \rho_o c_o u_{2A}(x) \end{bmatrix} = \begin{bmatrix} N_{1,1} & N_{1,2} & N_{1,3} & N_{1,4} \\ N_{2,1} & N_{2,2} & N_{2,3} & N_{2,4} \\ N_{3,1} & N_{3,2} & N_{3,3} & N_{3,4} \\ N_{4,1} & N_{4,2} & N_{4,3} & N_{4,4} \end{bmatrix} \begin{bmatrix} f_1 \\ f_2 \\ f_3 \\ f_4 \end{bmatrix}. \tag{62}$$

Using the two cases of $x = 0$ and $x = L_{C1}$ with Eq. (62) and rearranging the formula, the resultant relationship of the acoustic pressure and particle velocity between $x = 0$ and $x = L_{C1}$ becomes

$$\begin{bmatrix} p_2(0) \\ p_{2A}(0) \\ \rho_o c_o u_2(0) \\ \rho_o c_o u_{2A}(0) \end{bmatrix} = [B] \begin{bmatrix} p_2(L_{C1}) \\ p_{2A}(L_{C1}) \\ \rho_o c_o u_2(L_{C1}) \\ \rho_o c_o u_{2A}(L_{C1}) \end{bmatrix}, \tag{63}_1$$

where

$$[B] = [N(0)][N(L_{C1})]^{-1}. \tag{63}_2$$

To obtain the transform matrix between inlet $(x = 0)$ and outlet $(x = L_{C1})$ of the inner tubes, two boundary conditions for the outer tubers at $x = 0$ and $x = L_{C1}$ are calculated and listed below.

$$\frac{p_{2A}(0)}{-u_{2A}(0)} = -j\rho_o c_o \cot(kL_{A1}),$$

$$\frac{p_2(L_{C1})}{u_2(L_{C1})} = -j\rho_o c_o \cot(kL_{B1}). \tag{64}$$

By combining Eqs. (64) with Eq. (63) and developing them, the transfer matrix is deduced

$$\begin{bmatrix} p_2 \\ \rho_o c_o u_2 \end{bmatrix} = \begin{bmatrix} TPE_{1,1} & TPE_{1,2} \\ TPE_{2,1} & TPE_{2,2} \end{bmatrix} \begin{bmatrix} p_{3A} \\ \rho_o c_o u_{3A} \end{bmatrix}, \tag{65}_1$$

where

$$p_2 = p_2(0),$$

$$u_2 = u_2(0),$$

$$p_{3A} = p_{2A}(L_{C1}),$$

$$u_{3A} = u_{2A}(L_{C1}),$$

$$TPE_{1,1} = B_{1,1} + \left[\frac{B_{2,2} - jB_{4,2}\cot(kL_{A1})}{R_E}\right][B_{1,3}\rho_o c_o - jB_{1,1}\rho_o c_o \cot(kL_{B1})],$$

$$TPE_{1,2} = B_{1,4} + \left[\frac{B_{2,4} - jB_{4,4}\cot(kL_{A1})}{R_E}\right][B_{1,3}\rho_o c_o - jB_{1,1}\rho_o c_o \cot(kL_{B1})], \tag{65}_2$$

$$TPE_{2,1} = B_{3,2} + \left[\frac{B_{2,2} - jB_{4,2}\cot(kL_{A1})}{R_E}\right][B_{3,3}\rho_o c_o - B_{3,1}\rho_o c_o \cot(kL_{B1})],$$

$$TPE_{2,2} = B_{3,4} + \left[\frac{B_{2,4} - jB_{4,4}\cot(kL_{A1})}{R_E}\right][B_{3,3}\rho_o c_o - B_{3,1}\rho_o c_o \cot(kL_{B1})],$$

$$R_E = \rho_o c_o \left(B_{4,3} j \cot(kL_{A1}) + B_{4,1}\cot(kL_{A1})\cot(kL_{B1})\right.$$

$$\left. - B_{2,3} + B_{2,1} j \cot(kL_{B1})\right).$$

Acknowledgments

References

[1] MAGRAB E.B., *Environmental Noise Control,* John Wiley and Sons, New York 1975.

[2] SULLIVAN J.W., CROCKER M.J., *Analysis of concentric tube resonators having unpartitioned cavities,* Acous. Soc. Am., **64**, 207–215 (1978).

[3] SULLIVAN J.W., *A method of modeling perforated tube muffler components I: theory,* Acous. Soc. Am., **66**, 772–778 (1979).

[4] SULLIVAN J.W., *A method of modeling perforated tube muffler components II: theory,* Acous. Soc. Am., **66**, 779–788 (1979).

[5] JAYARAMAN K., YAM K., *Decoupling approach to modeling perforated tube muffler component*, Acous. Soc. Am., **69**, 2, 390–396 (1981).

[6] THAWANI P.T., JAYARAMAN K., *Modeling and applications of straight-through resonators*, Acous. Soc. Am., **73**, 4, 1387–1389 (1983).

[7] RAO K.N., MUNJAL M.L., *A generalized decoupling method for analyzing perforated element mufflers*, Nelson Acoustics Conference, Madison 1984.

[8] MUNJAL M.L, RAO K.N., SAHASRABUDHE A.D., *Aeroacoustic analysis of perforated muffler components*, Journal of Sound and Vibration, **114**, 2, 173–188 (1987).

[9] PEAT K.S., *A numerical decoupling analysis of perforated pipe silencer elements*, Journal of Sound and Vibration, **123**, 2, 199–212 (1988).

[10] CHANG Y.C., YEH L.J., CHIU M.C., *GA optimization on single-chamber muffler hybridized with extended tube under space constraints*, Archives of Acoustics, **29**, 4, 577–596 (2004).

[11] CHIU M.C., CHANG Y.C., *Shape optimization of multi-chamber cross-flow mufflers by SA optimization*, Journal of Sound Vibration, **312**, 3, 526–550 (2008).

[12] METROPOLIS A., ROSENBLUTH W., ROSENBLUTH M.N., TELLER H., TELLER E., *Equation of static calculations by fast computing machines*, J. Chem. Phys., **21**, 6, 1087–1092 (1953).

[13] KIRKPATRICK S., GELATT C.D., VECCHI M.P., *Optimization by simulated annealing*, Science, **220**, (4598), 671–680 (1983).

[14] MUNJAL M.L., *Acoustics of Ducts and Mufflers with Application to Exhaust and Ventilation System Design*, John Wiley and Sons, New York 1987.

[15] CHANG Y.C., YEH L.J., CHIU M.C., *Numerical studies on constrained venting system with side inlet/outlet mufflers by GA optimization*, Acta Acustica united with Acustica, **90**, 6, 1159–1169 (2004).

[16] NOLLE L., ARMSTRONG D.A., HOPGOOD A.A., WARE J.A., *Simulated annealing and genetic algorithms applied to finishing mill optimization for hot rolling of wide steel strip*, International of Knowledge-Based Intelligent Engineering System, **6**, 2, 104–111 (2002).

[17] SATHYANARAYANA Y., MUNJAL M.L., *A hybrid approach for aeroacoustic analysis of the engine exhaust system*, Applied Acoustics, **60**, 425–450 (2000).